J. Fluid Mech. (1992), *vol.* 236, *pp.* 635–664
Printed in Great Britain

Nonlinear spatial equilibration of an externally excited instability wave in a free shear layer

By LENNART S. HULTGREN

National Aeronautics and Space Administration, Lewis Research Center, Cleveland, OH 44135, USA

(Received 28 September 1990 and in revised form 13 September 1991)

A two-dimensional disturbance evolving from a strictly linear, finite-growth-rate instability wave with nonlinear effects first becoming important in the critical layer is considered. The analysis is carried out for a general weakly non-parallel mean flow using matched asymptotic expansions. The flow in the critical layer is governed by a nonlinear vorticity equation which includes a spatial-evolution term. As in Goldstein & Hultgren (1988), the critical layer ages into a quasi-equilibrium one and the initial exponential growth of the instability wave is converted into a weak algebraic growth during the roll-up process. This leads to a next stage of evolution where the instability-wave growth is simultaneously affected by mean-flow divergence and nonlinear critical-layer effects and is eventually converted to decay. Expansions for the various streamwise regions of the flow are combined into a single composite formula accounting for both shear-layer spreading and nonlinear critical-layer effects and good agreement with the experimental results of Thomas & Chu (1989), Freymuth (1966), and C.-M. Ho & Y. Zohar (1989, private communication) is demonstrated.

1. Introduction

Low-level external harmonic forcing of free shear layers between parallel streams produces spatially growing instability waves that are initially governed by linear dynamics. The local (linear) growth rate will ultimately be reduced, however, owing to the slow viscous spreading of the mean shear layer, and nonlinear effects can then first become important in a critical layer located at the transverse position where the phase velocity of the instability wave equals the mean velocity. In this situation, the perturbation flow outside the critical layer is essentially linear, but with the external instability-wave amplitude completely controlled by the critical-layer dynamics.

Goldstein & Leib (1988) (hereafter referred to as I) considered the case where the critical-layer balance is between spatial-evolution, linear- and nonlinear-convection terms, i.e. the nonlinearity can be characterized as strong but localized in the transverse coordinate. The presence of the spatial-evolution term in this balance means that the critical layer is an 'unsteady' one but with a slow streamwise coordinate in place of time. It will be referred to (as in I) as a non-equilibrium critical layer, however, in order to avoid any connotation of temporal evolution. This type of nonlinear critical layer occurs at the downstream position where the local linear growth rate is $O(\epsilon^{\frac{1}{2}})$, where ϵ is a measure of the local instability-wave amplitude. Its solution matches (in the matched asymptotics sense) onto the upstream finite-growth-rate, weakly non-parallel, linear instability wave, i.e. the proper initial (or upstream) conditions are applied in the nonlinear critical-layer theory. In I it was

assumed that the local Reynolds number R was large enough that viscous effects, including mean-flow spreading, could be ignored in the nonlinear (streamwise) region. Goldstein & Hultgren (1988) (hereafter referred to as II) incorporated a small amount of viscosity into the analysis of I. The local Reynolds number R was assumed to be $O(\epsilon^{-\frac{3}{2}})$ so that the viscous-diffusion term is of the same order of magnitude as the terms in the nonlinear critical-layer vorticity equation used in I. The relative importance of viscous to nonlinear effects in the critical layer is then determined by the parameter $\lambda = 1/\epsilon^{\frac{3}{2}}R$, while viscous effects play a purely passive role outside the critical layer. Their computations showed the vorticity roll-up to be initially similar to the inviscid calculations of I. However, once the nonlinear effects had generated sufficiently small scales, viscous effects asserted themselves and caused the vorticity distribution to diffuse into a simpler pattern more characteristic of an equilibrium critical layer. Their results also showed that viscosity keeps the nonlinear effects from driving the critical-layer phase jump, and thereby the local growth rate, to zero and hence allows the instability wave to continue its growth asymptotically far downstream. This produces an unbounded increase of the nonlinear terms in the critical-layer vorticity equation so that a new dominant critical-layer balance between linear and nonlinear convection terms is eventually achieved. This is analogous to the situation that was analysed by Benney & Bergeron (1969), but the specific asymptotic solution obtained in II turned out to be somewhat different and, in particular, has variable vorticity in the closed streamline region within the cat's-eye boundary.

It may at first seem surprising that no matter how large λ the problem in II becomes nonlinear sufficiently far downstream. This can be understood by realizing that the initial linear growth rate in the critical layer is independent of λ and that the growth rate is then rapidly reduced by nonlinear effects. A larger value of λ simply means that the growth rate is not reduced quite as fast because the relatively stronger viscous effects in a sense keep the problem linear for a longer streamwise distance. The instability wave can therefore, through continued growth, achieve the larger amplitude necessary for nonlinear effects now to come into play.

It was also shown in II that the initial exponential growth of the linear instability wave is converted into a weak algebraic growth as the critical layer ages into a quasi-equilibrium one and that this allows mean-flow divergence effects to alter the critical-layer structure before the instability wave achieves an $O(1)$ amplitude. It was found that the critical level moves a small distance across the shear layer in this next stage of evolution to maintain the quasi-equilibrium state against changes in mean flow and that the resulting instability-wave growth, therefore, is simultaneously affected by mean-flow divergence and nonlinear critical-layer effects. The growth rate goes to zero at the linear neutral point and the instability wave then begins to decay. The flow structure is shown schematically in figure 1 (reproduced from II).

The purpose of the present investigation is threefold. First, the analysis of II, which was restricted to a hyperbolic-tangent mean-velocity profile, is generalized to an arbitrary mean flow. This is accomplished in §§2 and 3. In §2, the nonlinear non-equilibrium critical-layer vorticity equation is derived and it is shown in Appendix C how the general problem can be transformed to the (now generic) problem studied in II. The next stage of evolution, where mean-flow divergence and nonlinear critical-layer effects both influence the evolution of the instability wave, is analysed in §3. Second, in §4, the streamwise composite solution introduced in I (formed from a weakly non-parallel linear solution valid on the slow mean-flow viscous spreading scale and the nonlinear critical-layer solution) is generalized to include viscosity and

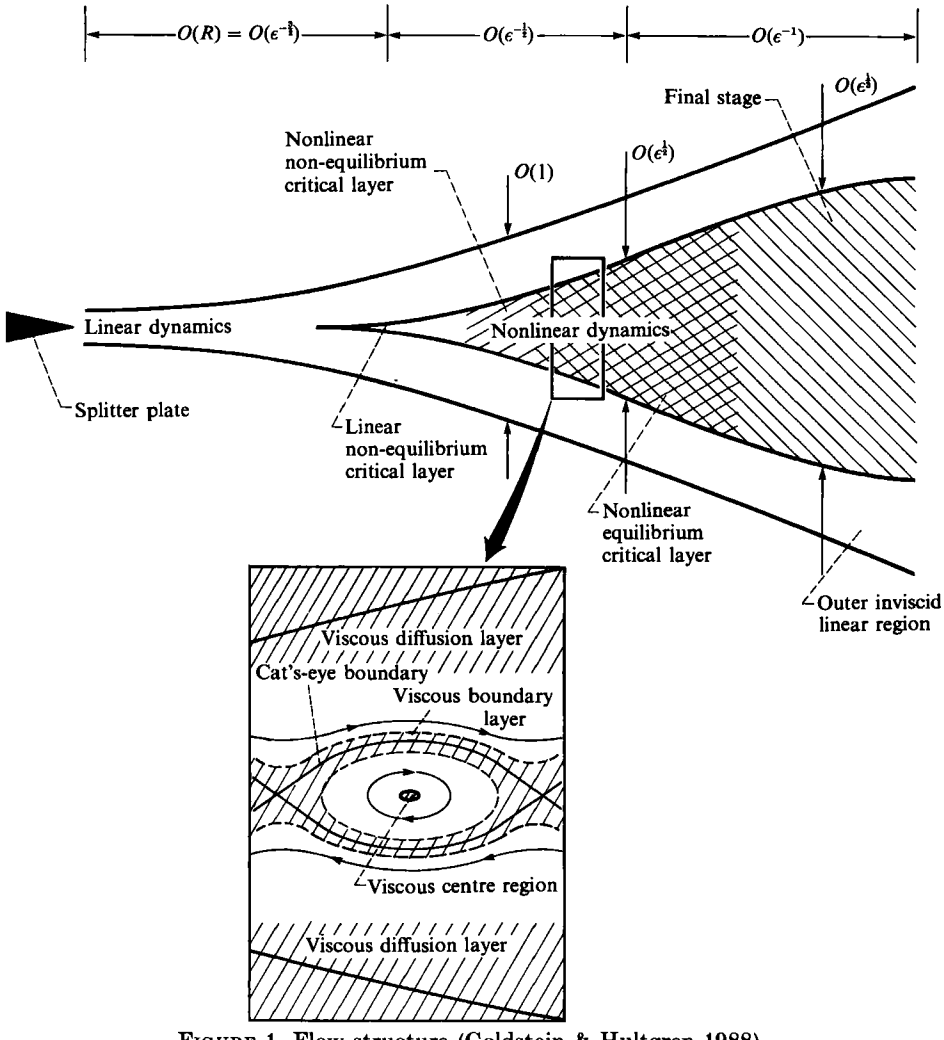

FIGURE 1. Flow structure (Goldstein & Hultgren 1988).

to be valid for a general velocity profile. It is found that the composite solution contains the next stage of evolution and, thus, is valid up to, and some distance beyond, the linear neutral point. The third, and perhaps most important, purpose of this paper is to make a first-principles comparison of results obtained by this type of asymptotic/numerical analysis with experiments. In a sense, the previously stated two purposes are simply prerequisites for this. The uniformly valid composite solution is shown in §5 to be in very good agreement with experimental results for a plane-jet shear layer (Thomas & Chu 1989), a circular-jet shear layer (Freymuth 1966), and a mixing layer behind a splitter plate (C.-M. Ho & Y. Zohar 1989, private communication).

2. Formulation of the nonlinear non-equilibrium critical-layer problem

As in I and II, consider a two-dimensional, incompressible and almost inviscid shear layer between two parallel streams with nominally uniform velocities $U_{1*} > U_{2*}$ (the star is used to denote dimensional quantities). In particular, consider the

streamwise region where nonlinear effects have become important, cf. figure 1. The streamwise and transverse coordinates x and y, the time t, and all velocities are non-dimensionalized by L_{v*}, L_{v*}/U_{A*}, and U_{A*}, respectively, where

$$2L_{v*} = (U_{1*} - U_{2*})/(\mathrm{d}U_*/\mathrm{d}y_*)_{\max}$$

is the vorticity thickness of the unexcited shear layer at a typical streamwise location, say $x = 0$, just upstream of the nonlinear region, and $U_{A*} = \frac{1}{2}(U_{1*} + U_{2*})$ is the average velocity of the streams. The origin of the y-coordinate is taken to be at the inflexion point of the undisturbed mean flow at $x = 0$.

The mean-flow Reynolds number, $R = L_{v*}U_{A*}/\nu$, where ν is the kinematic viscosity, is assumed large enough that the mean flow is nearly parallel and the shear-layer width (at least initially) increases only slowly over the long viscous scale

$$x_3 = x/R. \tag{2.1}$$

Upstream of the nonlinear region, the mean flow is essentially unaffected by the linear instability wave and its streamwise evolution can be determined from the laminar boundary-layer equation. In the same region, the instability wave can be described by inviscid, weakly non-parallel, linear stability theory and, assuming that it remains sufficiently small, its amplitude grows in the streamwise direction until, owing to the viscous mean-flow spreading, neutral stability is approached. As the local linear growth rate tends to zero, the leading-order inviscid stability problem becomes singular at the critical level, i.e. at the transverse location where the phase velocity of the instability wave equals the mean flow. This is indicative of a non-uniformity in the perturbation vorticity and that now the dynamics essentially is determined in a small transverse region. In this critical layer, the linear mean-flow convection of the perturbation vorticity can be balanced by spatial evolution (growth), viscous, or nonlinear effects, or a combination thereof. By themselves, these three possibilities would lead to an inviscid linear non-equilibrium critical layer with a thickness of the order of the small but non-zero growth rate, a viscous linear equilibrium critical layer of thickness $O(R^{-\frac{1}{3}})$, or an inviscid nonlinear equilibrium critical layer of thickness $O(\epsilon^{\frac{1}{2}})$, respectively, where ϵ is a measure of the local instability-wave amplitude. As first shown in I, the requirement that the near-neutral nonlinear solution matches onto the upstream strictly linear, finite-growth-rate instability wave implies that the linear growth rate at the beginning of the nonlinear region must be $O(\epsilon^{\frac{1}{2}})$. This scaling represents a distinguished limit that allows both spatial evolution and nonlinear effects to enter the critical-layer vorticity balance and has a linear non-equilibrium critical-layer region (cf. figure 1) as an overlap domain between the upstream finite-growth-rate linear region and the near-neutral nonlinear region. Consequently, it is assumed that in the nonlinear streamwise region

$$S = S_0 + \epsilon^{\frac{1}{2}}S_1, \quad S_1 < 0, \quad S_1 = O(1), \tag{2.2}$$

where $S = \omega_{e*}L_{v*}/U_{A*}$ is the local Strouhal number, $S_0 = \alpha_0 U_c$ is its local neutral value based on linear inviscid parallel-flow stability theory, ω_{e*} is the excitation angular frequency, α_0 is the local neutral wavenumber and U_c is the velocity at the inflexion point of the undisturbed mean flow at $x = 0$. S_0 and S_1 are taken to be constant at present, but will be allowed to vary on the long viscous scale x_3 when, later, the streamwise composite solution is introduced. Furthermore, as in II, the parameter

$$\lambda = 1/\epsilon^{\frac{3}{2}}R \tag{2.3}$$

describing the relative importance of viscous to nonlinear effects in the critical layer is taken to be $O(1)$. Viscous effects then enter into the critical-layer vorticity balance but are purely passive in the main part of the shear layer. The analysis of II shows that critical-layer effects cause changes in the flow on the scale of the slow streamwise variable

$$x_1 = \epsilon^{\frac{1}{2}} x, \tag{2.4}$$

and that it is sufficient to use the (local) Taylor series expansion of the basic-flow velocity for the purpose of studying its changes on the nonlinear critical-layer streamwise lengthscale (2.4). The analysis here need only be uniformly valid on the scale x_1 but not on the slower scale x_3, cf. figure 1.

As in I and II, the solution in the nonlinear streamwise region will now be expanded separately outside and inside the critical layer. Matching (in the transverse direction) of these expansions, which also involves equating the so-called velocity jump across the critical layer as given by the two expansions, will then lead to a nonlinear non-equilibrium critical-layer problem which completely determines the external instability-wave amplitude.

As in I and II, the solution outside the critical layer is expanded as

$$\psi = \psi_0(y) + \epsilon\psi_1(\zeta, y, x_1) + \epsilon^{\frac{3}{2}}\psi_{\frac{3}{2}} + \epsilon^2\psi_2 + \epsilon^{\frac{5}{2}}\psi_{\frac{5}{2}} + O(\epsilon^3). \tag{2.5}$$

ψ_0 is the zeroth-order term in the Taylor-series expansion for the basic flow, which is determined by the imposed upstream profile and by the previous slow development on the long viscous scale $x_3 = x/R$. The $\psi_{n/2}$ for $n \geqslant 2$ are functions of y, the slow variable x_1, and

$$\zeta = x - St/\alpha_0, \tag{2.6}$$

the streamwise coordinate in a reference frame moving with the actual phase velocity of the linear instability wave. The equations governing the first few $\psi_{n/2} (n \geqslant 2)$ are given in Appendix A.

As in II, the $O(\epsilon)$ term, ψ_1, in the expansion (2.5) is the sum of the second term in the basic-flow Taylor series expansion and the (neutral) linear instability wave solution, i.e.

$$\psi_1 = 2\lambda x_1 G(y) + \mathrm{Re}\,[A^\dagger(x_1)\,\hat{\phi}_1(y)\,\mathrm{e}^{\mathrm{i}\alpha_0\zeta}], \tag{2.7}$$

where the mean-flow change term $G(y)$ and the slowly varying amplitude function $A^\dagger$ are ultimately determined by the $O(\epsilon^{\frac{3}{2}})$ problem. The higher $\psi_{n/2}$ are of the form

$$\psi_{n/2} = \mathrm{Re}\left[\sum_{m=0}^{+\infty} \Phi_{n/2}^{(m)}(y, x_1)\,\mathrm{e}^{\mathrm{i}m\alpha_0\zeta}\right] \quad \text{for} \quad n = 3, 4, \ldots. \tag{2.8}$$

Substitution of (2.7) and (2.8) into the governing equations (see Appendix A) leads to a sequence of equations of which the first two for the fundamental component and its harmonics are

$$\mathrm{L}_1\hat{\phi}_1 = 0, \tag{2.9}$$

$$\mathrm{L}_m\,\Phi_{\frac{3}{2}}^{(m)} = -\mathrm{i}\delta_{m1}\left[2\alpha_0\frac{\mathrm{d}A^\dagger}{\mathrm{d}x_1} - \frac{U''}{\alpha_0(U-U_c)^2}\left(U_c\frac{\mathrm{d}A^\dagger}{\mathrm{d}x_1} - \mathrm{i}S_1A^\dagger\right)\right]\hat{\phi}_1, \quad m > 0, \tag{2.10}$$

where

$$\mathrm{L}_m = \mathrm{D}^2 - m^2\alpha_0^2 - \frac{U''}{U-U_c}, \tag{2.11}$$

$\mathrm{D} = \mathrm{d}/\mathrm{d}y$, and δ_{ij} is the Kronecker tensor. Equations (2.9) (the Rayleigh equation for a regular neutral disturbance) and (2.10) are to be solved subject to the boundary conditions $(\hat{\phi}_1, \Phi_{\frac{3}{2}}^{(m)}) \to 0$ as $|y| \to +\infty$ and a normalization condition, say $\hat{\phi}_1(0) = 1$.

$G(y)$ and $\Phi_{\frac{3}{2}}^{(0)}$ are determined by the ζ-independent part of the $O(\epsilon^{\frac{3}{2}})$ and $O(\epsilon^2)$ problems, respectively, and are given in Appendix A.

For small values of y, i.e. as the critical layer is approached, $\hat{\phi}_1$ can be expressed in terms of the Tollmien solutions to obtain

$$\hat{\phi}_1 = 1+\tfrac{1}{2}\left(\alpha_0^2+\frac{U_c'''}{U_c'}\right)y^2+O(y^3)+b_1[y+O(y^3)], \tag{2.12}$$

where $b_1 = \hat{\phi}_1'(0)$ and can be easily determined from a numerical solution of (2.9). It follows from (2.10) and (2.12) that for small values of y

$$\Phi_{\frac{3}{2}}^{(m)} = a_{\frac{3}{2}}^{(m)}+b_{\frac{3}{2}}^{(m)\pm}y+\delta_{m1}\frac{\mathrm{i}U_c'''}{\alpha_0 U_c'^2}\left(U_c\frac{\mathrm{d}A^\dagger}{\mathrm{d}x_1}-\mathrm{i}S_1A^\dagger\right)y\ln|y|+O(y^2), \quad m>0, \tag{2.13}$$

where the $\pm$ superscript indicates different values for $y \gtrless 0$.

Multiplication of (2.10) for $m=1$ with $\hat{\phi}_1$, subtraction of $\Phi_{\frac{3}{2}}^{(1)}$ times (2.9) from the resulting equation, followed by integration from $-\infty$ to $-\delta$ and δ to $+\infty$, then taking the limit of $\delta\to 0+$ and using the boundary conditions at infinity and the small-y results (2.12) and (2.13) leads to the following solvability condition for (2.10):

$$b_{\frac{3}{2}}^{(1)+}-b_{\frac{3}{2}}^{(1)-} = 2\mathrm{i}\alpha_0\frac{\mathrm{d}A^\dagger}{\mathrm{d}x_1}J_1-\mathrm{i}\alpha_0\left(U_c\frac{\mathrm{d}A^\dagger}{\mathrm{d}x_1}-\mathrm{i}S_1A^\dagger\right)J_2, \tag{2.14}$$

where

$$J_1 = \int_{-\infty}^{+\infty}\hat{\phi}_1^2\,\mathrm{d}y, \tag{2.15}$$

$$J_2 = \frac{1}{\alpha_0^2}\oint_{-\infty}^{+\infty}\frac{U''\hat{\phi}_1^2\,\mathrm{d}y}{(U-U_c)^2}, \tag{2.16}$$

and $\oint$ denotes a Cauchy principal value integral. Note that $J_2 = 0$ for antisymmetric mean velocity profiles, e.g. the hyperbolic-tangent profile considered in I and II. Equation (2.14) gives the so-called velocity jump across the critical layer as (formally) computed from the outer solution. Its imaginary part is usually referred to as the phase jump.

Further details about the behaviour of the outer solution in neighbourhood of the critical layer can be found in Appendix A. As in I and II, the scaled transverse coordinate

$$Y = y/\epsilon^{\frac{1}{2}} \tag{2.17}$$

is now introduced to describe the solution in the critical layer. The stream function in the critical layer is also expanded as

$$\psi = \epsilon^{\frac{1}{2}}U_c\,Y+\epsilon(\Psi_0+\epsilon^{\frac{1}{2}}\Psi_{\frac{1}{2}}+\epsilon\ln\epsilon^{\frac{1}{2}}\Psi_{1L}+\epsilon\Psi_1+\ldots), \tag{2.18}$$

where the Ψ_n are functions of ζ, Y, and x_1 only. Ψ_0 to Ψ_{1L} are simply given by the corresponding terms in the inner limit of the outer solution (obtained by substituting (2.17) into (2.5) and re-expanding the result with the inner variable Y held fixed) and are given in Appendix B. Ψ_1, the first non-trivial term in (2.18), is determined by the viscous critical-layer vorticity equation

$$\left[U_c\frac{\partial}{\partial x_1}+\left(U_c'\,Y-\frac{S_1}{\alpha_0}\right)\frac{\partial}{\partial\zeta}-\mathrm{Re}\,(\mathrm{i}\alpha_0A^\dagger\mathrm{e}^{\mathrm{i}\alpha_0\zeta})\frac{\partial}{\partial Y}\right]\Omega_1-\lambda\frac{\partial^2\Omega_1}{\partial Y^2} = 0, \tag{2.19}$$

where

$$\Omega_1 = \frac{\partial^2\Psi_1}{\partial Y^2}-\mathrm{Re}\,(\alpha_0^2A^\dagger\mathrm{e}^{-\mathrm{i}\alpha_0\zeta}) \tag{2.20}$$

and the total critical-layer vorticity is given by $-(U_c'+\epsilon\Omega_1)+O(\epsilon^{\frac{3}{2}})$.

Integration of (2.20) with respect to Y from $-M$ to M, letting $M \to \infty$, and using the inner limit of the outer solution produces the matching condition

$$b_{\frac{3}{2}}^{(m)+} - b_{\frac{3}{2}}^{(m)-} = \frac{\alpha_0}{\pi} \int_{-\infty}^{+\infty} \int_0^{2\pi/\alpha_0} Q^\dagger \, \mathrm{e}^{-\mathrm{i}m\alpha_0\zeta} \, \mathrm{d}\zeta \, \mathrm{d}Y, \tag{2.21}$$

where

$$Q^\dagger = \Omega_1 - U_c''' \left[\tfrac{1}{2} Y^2 + \frac{\lambda x_1}{U_c} + \frac{1}{U_c} Re\,(A^\dagger \mathrm{e}^{\mathrm{i}\alpha_0\zeta}) \right] \tag{2.22}$$

is minus the part of the $O(\epsilon)$ critical-layer vorticity that vanishes as $|Y| \to +\infty$. For $m = 1$, equation (2.21) gives the velocity jump across the critical layer as (formally) computed from the critical-layer solution. Equating the expressions for the velocity jump involving the outer and inner solutions, respectively, leads to the matching condition

$$\int_{-\infty}^{+\infty} \int_0^{2\pi/\alpha_0} Q^\dagger \, \mathrm{e}^{-\mathrm{i}\alpha_0\zeta} \, \mathrm{d}\zeta \, \mathrm{d}Y = \mathrm{i}\pi \left[2J_1 \frac{\mathrm{d}A^\dagger}{\mathrm{d}x_1} - J_2 \left(U_c \frac{\mathrm{d}A^\dagger}{\mathrm{d}x_1} - iS_1 A^\dagger \right) \right]. \tag{2.23}$$

Equations (2.19)–(2.23), together with the boundary condition that $Q^\dagger \to 0$ as $|Y| \to +\infty$, defines the nonlinear critical-layer problem.

Note that for $m > 1$, equation (2.21) determines the amplitude of the $O(\epsilon^{\frac{3}{2}})$ higher harmonics in the outer flow. This problem, i.e. (2.10) subject to the boundary conditions $\Phi_{\frac{3}{2}}^{(m)} \to 0$ as $|y| \to +\infty$ and to (2.21), all for $m > 1$, is a well-posed problem as long as $b_{\frac{3}{2}}^{(m)} \neq b_{\frac{3}{2}}^{(m)-}$ for all $m > 1$. If this is true then the $b_{\frac{3}{2}}^{(m)\pm}$ can each be determined in terms of the corresponding $a_{\frac{3}{2}}^{(m)}$ from the conditions at $y = \pm\infty$ (in general through a numerical solution of the problem) and (2.21) then sets the amplitude of this solution, i.e. the higher harmonics are forced by the critical-layer nonlinearity. If, however, $b_{\frac{3}{2}}^{(m)+} = b_{\frac{3}{2}}^{(m)-}$ for some m, then that harmonic is also a neutral eigensolution to the Rayleigh stability problem and this case must be treated separately because nonlinear interaction of the two eigensolutions is then possible in the critical layer(s) (e.g. Leib & Goldstein 1989). This is not likely to occur for a monotonic mean-flow profile (which only has one critical layer), however.

As $x_1 \to -\infty$, the solution approaches that of a linear growth critical layer and it can easily be shown that the proper initial condition for (2.19)–(2.23) is

$$A^\dagger \to A_0^\dagger \exp\left[-\tfrac{1}{2} \int_0^{x_1} S_1 \sigma^\dagger \, \mathrm{d}x_1 \right], \tag{2.24}$$

where

$$\sigma^\dagger = \gamma\sigma, \tag{2.25}$$

$$\gamma = -U_c'''/\alpha_0^2 U_c' |U_c'| J_1, \tag{2.26}$$

$$\sigma \equiv \sigma_r + \mathrm{i}\sigma_1 = (\pi + \mathrm{i}\mu)/(\chi + \tfrac{1}{2}\mathrm{i}\pi\bar{U}), \tag{2.27}$$

$$\mu = J_2/\gamma J_1, \tag{2.28}$$

$$\chi = 1 - \tfrac{1}{2}\mu\bar{U} \tag{2.29}$$

$$\bar{U} = \gamma U_c. \tag{2.30}$$

Strictly speaking, the integrand in (2.24) is constant on the streamwise scale x_1 considered here. It is advantageous to write the upstream conditions for the nonlinear solution in the form (2.24) for the later introduction of a streamwise composite solution, however. Analogous comments also hold for equations (2.31), (2.36), (2.37), and (2.40) below.

By introducing the rescaled variables

$$\bar{x} = -\tfrac{1}{2}\int_0^{x_1} \gamma S_1 \, \mathrm{d}x_1 + \bar{x}_0, \tag{2.31}$$

$$X = \alpha_0 \zeta + X_0, \tag{2.32}$$

$$\eta = (\alpha_0 U_c' Y - S_1)/(-\tfrac{1}{2}\bar{U}S_1), \tag{2.33}$$

$$A = [\alpha_0^2 U_c'/(-\tfrac{1}{2}\bar{U}S_1)^2] A^\dagger \mathrm{e}^{-\mathrm{i}X_0}, \tag{2.34}$$

$$Q = -[(\alpha_0 U_c')^2 \bar{U}/2U_c'''(-\tfrac{1}{2}\bar{U}S_1)^2] Q^\dagger, \tag{2.35}$$

where $\bar{x}_0$ and X_0 are given by

$$\int_0^{\bar{x}_0} \sigma_r \, \mathrm{d}\bar{x} = \ln\left[\frac{\alpha_0^2 U_c' |A_0^\dagger|}{(-\tfrac{1}{2}\bar{U}S_1)^2}\right], \tag{2.36}$$

$$X_0 = \arg A_0^\dagger - \int_0^{\bar{x}_0} \sigma_i \, \mathrm{d}\bar{x}_0, \tag{2.37}$$

and

$$\bar{\lambda} = [(\alpha_0 U_c')^2/(-\tfrac{1}{2}\bar{U}S_1)^3]\lambda, \tag{2.38}$$

the nonlinear non-equilibrium critical-layer problem, i.e. (2.19)–(2.23), and the associated initial and boundary conditions are converted into the following scaled critical-layer problem:

$$\left[\frac{\partial}{\partial \bar{x}} + \eta\frac{\partial}{\partial X} - \mathrm{Re}\,(\mathrm{i}A\,\mathrm{e}^{\mathrm{i}X})\frac{\partial}{\partial \eta} - \bar{\lambda}\frac{\partial^2}{\partial \eta^2}\right] Q = \mathrm{Re}\left[\left(\tfrac{1}{2}\bar{U}\frac{\mathrm{d}A}{\mathrm{d}\bar{x}} + \mathrm{i}A\right)\mathrm{e}^{\mathrm{i}X}\right], \tag{2.39}$$

subject to the initial, boundary, and jump conditions

$$A \to \exp\left(\int_0^{\bar{x}} \sigma \, \mathrm{d}\bar{x}\right) \quad \text{as} \quad \bar{x} \to -\infty, \tag{2.40}$$

$$Q \to 0 \quad \text{as} \quad |\eta| \to \infty, \tag{2.41}$$

$$\frac{1}{\pi}\int_{-\infty}^{+\infty}\int_0^{2\pi} \mathrm{e}^{-\mathrm{i}X} Q \, \mathrm{d}X \, \mathrm{d}\eta = \mathrm{i}\left(\chi\frac{\mathrm{d}A}{\mathrm{d}\bar{x}} - \mathrm{i}\mu A\right). \tag{2.42}$$

In view of (2.29), this problem depends on the three independent parameters $\bar{U}$, $\bar{\lambda}$, and μ. $\bar{U}$ is a scaled average mean-flow velocity in the critical layer (measured in the laboratory frame of reference); $\bar{\lambda}$ is a rescaled λ which in view of (2.2), (2.3), and (2.38) could be thought of as based on the detuning from the local neutral conditions rather than the amplitude; and μ is π times the ratio of the real and imaginary parts of the derivative of the wavenumber with respect to the phase velocity (both from linear inviscid theory) evaluated at the neutral point, which vanishes for antisymmetric mean profiles such as the one used in I and II, and can be interpreted as a mean-flow symmetry parameter.

The nonlinear non-equilibrium critical-layer problem, i.e. (2.39)–(2.42), can, however, be converted into the scaled critical-layer problem for the hyperbolic-tangent mean-flow problem studied in II by introducing new variables as described in Appendix C. Thus, the nonlinear non-equilibrium critical-layer problem studied in II, which is of the form (2.39)–(2.42) but with $\mu = 0$, therefore applies to an arbitrary mean-flow profile provided the meaning of $\bar{U}$ and $\bar{\lambda}$ in II are suitably generalized. (The form (2.39)–(2.42) actually turns out to be better suited to the numerical streamwise composite-solution procedure to be employed later, however.) The results of II showed that, no matter what the size of the parameter $\bar{\lambda}$, eventually the amplitude A exhibits algebraic growth and the critical layer is converted into a

primarily inviscid quasi-equilibrium one as $\bar{\lambda}\bar{x}$ becomes large. The asymptotic solution to the nonlinear non-equilibrium critical-layer problem constructed in that limit in II is, of course, also valid in the general case analysed here and it is briefly described in Appendix C.

3. The next stage of evolution

As shown in II, the relatively slow algebraic growth of the instability wave as $x_1 \to +\infty$ allows the viscous mean-flow divergence eventually to alter the critical-layer structure and thereby induce a correction to the local growth rate before the instability-wave amplitude becomes $O(1)$. When

$$x_2 = \epsilon^{\frac{1}{2}} x_1 = \epsilon x = \epsilon^{-\frac{1}{2}} x_3 \tag{3.1}$$

is $O(1)$, this correction becomes of the same order of magnitude as the local growth rate and the non-equilibrium nonlinear critical-layer expansion will no longer be valid. Since the actual instability-wave amplitude is still only $O(\epsilon^{\frac{3}{4}})$ in this streamwise region, the nonlinear effects are again confined to a narrow critical layer, now of thickness $O(\epsilon^{\frac{1}{3}})$, while the flow behaves linearly in the main part of the shear layer. As in II, the critical layer now moves an $O(\epsilon^{\frac{1}{2}})$ distance, i.e. a small fraction of its width, across the shear layer in order to remain in the quasi-equilibrium state achieved asymptotically in the previous stage.

For $x_2 = O(1)$, the expansion in the main part of the shear layer, i.e. for $y = O(1)$, is to a large extent a simple reordering of the corresponding expansion in §2 and, as in II, is of the form

$$\psi = \psi_0 + \epsilon^{\frac{1}{3}} 2\lambda x_2 G(y) + \epsilon^{\frac{2}{3}} A_\infty(x_2)\, \hat{\phi}_1(y) \cos\left(\alpha_0 \zeta - \frac{\Theta_\infty(x_2)}{\epsilon^{\frac{1}{3}}}\right) + \epsilon(\lambda x_2)^2 G^{(2)}(y)$$
$$+ \epsilon^{\frac{7}{6}} \psi_{\frac{7}{6}} + \epsilon^{\frac{4}{3}} \psi_{\frac{4}{3}} + \epsilon^{\frac{3}{2}} (\lambda x_2)^3 G^{(3)}(y) + \epsilon^{\frac{5}{3}} \psi_{\frac{5}{3}} + \ldots, \tag{3.2}$$

where ζ is given by (2.6); ψ_0 is the basic flow of §2; G, $G^{(2)}$ and $G^{(3)}$ are the y-dependent coefficients in the Taylor-series expansion of the basic-flow stream function; $\hat{\phi}_1$ is the neutral eigenfunction; and A_∞ and Θ_∞ are real functions of x_2.

In order for the downstream expansion (3.2) to match onto the solution in the preceding non-equilibrium region, it follows from (2.5), (2.7), (C 1)–(C 12), and (3.1) that as $x_2 \to 0$

$$A_\infty \to a_\infty \left(\frac{U_c'}{\alpha_0^2}\right)^{\frac{1}{3}} \left(-\tfrac{1}{2}\lambda \int_0^{x_2} \frac{\gamma S_1}{\chi^2}\, \mathrm{d}x_2\right)^{\frac{2}{3}}, \tag{3.3}$$

$$\Theta_\infty' \to -\frac{\gamma}{2\chi^2}(\theta_\infty' - \chi\mu) S_1, \tag{3.4}$$

where γ, μ, χ, a_∞ and θ_∞' are defined by (2.26), (2.28), (2.29), (C 11) and (C 12), and detailed formulae for the latter two quantities are given in II.

The $O(\epsilon^{\frac{7}{6}})$, $O(\epsilon^{\frac{4}{3}})$ and $O(\epsilon^{\frac{5}{3}})$ terms are now of the form

$$\psi_{\frac{7}{6}} = \Phi_{\frac{7}{6}}(y, x_2) \cos\left(\alpha_0 \zeta - \frac{\Theta_\infty(x_2)}{\epsilon^{\frac{1}{2}}}\right), \tag{3.5}$$

$$\psi_{\frac{4}{3}} = \Phi_{\frac{4}{3}}^{(0)}(y, x_2) + \Phi_{\frac{4}{3}}^{(2)}(y, x_2) \cos\left[2\left(\alpha_0 \zeta - \frac{\Theta_\infty(x_2)}{\epsilon^{\frac{1}{3}}}\right)\right], \tag{3.6}$$

$$\psi_{\frac{5}{3}} = \Phi_{\frac{5}{3}}^{(c)} \cos\left(\alpha_0 \zeta - \frac{\Theta_\infty(x_2)}{\epsilon^{\frac{1}{2}}}\right) + \Phi_{\frac{5}{3}}^{(s)} \sin\left(\alpha_0 \zeta - \frac{\Theta_\infty(x_2)}{\epsilon^{\frac{1}{2}}}\right), \tag{3.7}$$

where the two terms in (3.7) will be referred to as the in-phase and out-of-phase parts, respectively. Just as in II, neither $\Phi_{\frac{1}{3}}^{(0)}$, $\Phi_{\frac{1}{3}}^{(2)}$ nor the in-phase term in (3.7) play a role in the determination of the amplitude and phase to the order of approximation of the analysis and, for simplicity of presentation, are therefore ignored in what follows. $\Phi_{\frac{7}{6}}$ and $\Phi_{\frac{5}{3}}^{(s)}$ are determined by

$$\mathrm{L}_1 \Phi_{\frac{7}{6}} = -\left[2\alpha_0 \Theta'_\infty - \frac{U''}{\alpha_0 (U-U_c)^2}(U_c \Theta'_\infty + S_1) + \frac{2\lambda x_2}{U-U_c}\left(\frac{G'U''}{U-U_c} - G'''\right)\right] A_\infty \hat{\phi}_1, \quad (3.8)$$

$$\mathrm{L}_1 \Phi_{\frac{5}{3}}^{(s)} = \left[2\alpha_0 - \frac{U_c U''}{\alpha_0 (U-U_c)^2}\right] A'_\infty \hat{\phi}_1. \quad (3.9)$$

The boundary conditions for (3.8) and (3.9) are that $(\Phi_{\frac{7}{6}}, \Phi_{\frac{5}{3}}^{(s)}) \to 0$ as $|y| \to +\infty$. It follows from (2.12), (3.8), and (3.9) that for small values of y

$$\Phi_{\frac{7}{6}} = a_{\frac{7}{6}} + b_{\frac{7}{6}}^{\pm}\, y + \frac{A_\infty}{\alpha_0}\left[(U_c \Theta'_\infty + S_1)\frac{U'''_c}{U'^2_c} - \alpha_0 \lambda x_2 \left(\frac{U'''_c}{U_c^2} - \frac{U_c^{iv}}{U_c U'_c}\right)\right] y \ln|y| + O(y^2), \quad (3.10)$$

$$\Phi_{\frac{5}{3}}^{(s)} = a_{\frac{5}{3}}^{(s)} + b_{\frac{5}{3}}^{(s)\pm}\, y - \frac{U_c U'''_c}{\alpha_0 U'^2_c} A'_\infty\, y \ln|y| + O(y^2). \quad (3.11)$$

The solvability conditions (constructed as in §2) for (3.8) and (3.9) become

$$b_{\frac{7}{6}}^{+} - b_{\frac{7}{6}}^{-} = \alpha_0 A_\infty [2\Theta'_\infty J_1 - (U_c \Theta'_\infty + S_1) J_2 + 2\lambda x_2 J_5], \quad (3.12)$$

$$b_{\frac{5}{3}}^{(s)+} - b_{\frac{5}{3}}^{(s)-} = -\alpha_0 A'_\infty (2J_1 - U_c J_2), \quad (3.13)$$

where J_1 and J_a are given by (2.15) and (2.16), respectively, and

$$J_5 = \frac{1}{\alpha_0} \int_{-\infty}^{+\infty} \left(\frac{G'U''}{U-U_c} - G'''\right) \frac{\hat{\phi}_1^2}{U-U_c}\, \mathrm{d}y. \quad (3.14)$$

Equations (3.12) and (3.13) determine the real and imaginary parts of the velocity jump across the critical layer to leading order, respectively.

The critical-layer stream function is now expanded as

$$\psi = \epsilon^{\frac{1}{3}} U_c \bar{Y} + \epsilon^{\frac{1}{2}} 2\lambda x_2 c_1^{(0)} U_c + \epsilon^{\frac{2}{3}}(\Psi_0 + \epsilon^{\frac{1}{6}} \Psi_{\frac{1}{6}} + \epsilon^{\frac{1}{3}} \Psi_{\frac{1}{3}} + \epsilon^{\frac{1}{2}} \Psi_{\frac{1}{2}} + \epsilon^{\frac{2}{3}} \Psi_{\frac{2}{3}} + \epsilon^{\frac{5}{6}} \ln \epsilon \Psi_{\frac{5}{6}L} + \epsilon^{\frac{5}{6}} \Psi_{\frac{5}{6}} + \epsilon \Psi_1 + \epsilon^{\frac{7}{6}} \Psi_{\frac{7}{6}} + \epsilon^{\frac{4}{3}} \Psi_{\frac{4}{3}} \ldots), \quad (3.15)$$

where

$$\bar{Y} = y/\epsilon^{\frac{1}{3}} \quad (3.16)$$

is a stretched transverse coordinate. The $O(\epsilon^{\frac{1}{3}})$ and $O(\epsilon^{\frac{1}{2}})$ terms and Ψ_0 to $\Psi_{\frac{5}{6}L}$ are simply re-expansions of the outer (main-region) solution. Only $\Psi_{\frac{5}{6}}$ and the out-of-phase part of $\Psi_{\frac{4}{3}}$ of the remaining non-trivial terms in (3.15) play a dynamically significant role in determining the instability amplitude and phase to lowest order and they are determined by

$$\mathscr{L}_e \Omega_{\frac{5}{6}} = -\frac{U'''_c}{U'_c}(U_c \Theta'_\infty + S_1 - 2\lambda x_2 c_1^{(0)} U'_c) A_\infty \sin\left(\alpha_0 \zeta - \frac{\Theta_\infty(x_2)}{\epsilon^{\frac{1}{2}}}\right), \quad (3.17)$$

$$\mathscr{L}_e \Omega_{\frac{4}{3}}^{(s)} = \lambda \frac{\partial^2 \Omega_{\frac{5}{6}}}{\partial \bar{Y}^2} - \frac{U'''_c U_c}{U'_c} A'_\infty \cos\left(\alpha_0 \zeta - \frac{\Theta_\infty(x_2)}{\epsilon^{\frac{1}{2}}}\right), \quad (3.18)$$

where $\mathscr{L}_e$ is the equilibrium critical-layer vorticity operator

$$\mathscr{L}_e = U'_c \bar{Y} \frac{\partial}{\partial \zeta} + \alpha_0 A_\infty \sin\left(\alpha_0 \zeta - \frac{\Theta_\infty(x_2)}{\epsilon^{\frac{1}{2}}}\right) \frac{\partial}{\partial \bar{Y}}, \quad (3.19)$$

and $\Omega_{\frac{5}{6}} = \partial^2 \Psi_{\frac{5}{6}}/\partial \bar{Y}^2$ and $\Omega^{(s)}_{\frac{4}{3}} = \partial^2 \Psi^{(s)}_{\frac{4}{3}}/\partial \bar{Y}^2$ are minus the $O(\epsilon^{\frac{5}{6}})$ and minus the out-of-phase component of the $O(\epsilon^{\frac{4}{3}})$ critical-layer vorticity.

The solutions to (3.17)–(3.19) must satisfy the transverse boundary conditions

$$\Omega_{\frac{5}{6}} \to \lambda x_2 \left(2c_1^{(0)} U_c''' + \frac{U_c^{iv}}{U_c} - \frac{U_c' U_c'''}{U_c^2} \right) \bar{Y}, \tag{3.20}$$

$$\Omega^{(s)}_{\frac{4}{3}} \to 0, \tag{3.21}$$

as $|\bar{Y}| \to \infty$, together with the integral constraints

$$\frac{1}{2\pi} \int_{-\infty}^{+\infty} \int_0^{2\pi/\alpha_0} \Omega_{\frac{5}{6}} \cos\left(\alpha_0 \zeta - \frac{\Theta_\infty(x_2)}{\epsilon^{\frac{1}{2}}} \right) \mathrm{d}\zeta \, \mathrm{d}\bar{Y}$$

$$= A_\infty [(J_1 - \tfrac{1}{2} U_c J_2) \Theta'_\infty - \tfrac{1}{2} S_1 J_2 + \lambda x_2 J_5], \tag{3.22}$$

$$\frac{1}{2\pi} \int_{-\infty}^{+\infty} \int_0^{2\pi/\alpha_0} \Omega^{(s)}_{\frac{4}{3}} \sin\left(\zeta - \frac{\Theta_\infty(x_2)}{\epsilon^{\frac{1}{2}}} \right) \mathrm{d}\zeta \, \mathrm{d}\bar{Y} = -A'_\infty (J_1 - \tfrac{1}{2} U_c J_2), \tag{3.23}$$

in order to match with the outer expansion (3.2).

As in II, this boundary-value problem (3.17)–(3.23) can effectively be converted into a quasi-equilibrium nonlinear critical-layer problem like the one in §5 of II and the final results for the amplitude and phase are

$$A_\infty = a_\infty \left(\frac{U_c'}{\alpha_0^2} \right)^{\frac{1}{3}} \left(-\tfrac{1}{2} \lambda \int_0^{x_2} \frac{\gamma S_1^{(A)}}{\chi^2} \mathrm{d}x_2 \right)^{\frac{2}{3}}, \tag{3.24}$$

$$\Theta'_\infty = -\alpha_1 - \frac{\gamma}{2\chi^2} (\theta'_\infty - \chi \mu) S_1^{(A)}, \tag{3.25}$$

where

$$\alpha_1 = \frac{\lambda x_2}{J_1} \left[J_5 - \frac{\alpha_0 U_c'}{2U_c'''} \left(\frac{U_c' U_c'''}{U_c^2} - \frac{U_c^{iv}}{U_c} \right) J_2 \right], \tag{3.26}$$

$$S_1^{(A)} = S_1 - \frac{\lambda x_2}{J_1} \left[\frac{\alpha_0 U_c'}{U_c'''} \left(\frac{U_c' U_c'''}{U_c^2} - \frac{U_c^{iv}}{U_c} \right) (J_1 - \tfrac{1}{2} U_c J_2) + U_c J_5 \right]. \tag{3.27}$$

A relatively straightforward perturbation calculation based on the Rayleigh linear stability problem with the base flow given by the first two terms in (3.2) (in order to incorporate a weak mean-flow divergence) shows that α_1 is the $O(\epsilon^{\frac{1}{2}})$ change in the neutral wavenumber due to the slowly changing local conditions and $S_1^{(A)}$ is the actual $O(\epsilon^{\frac{1}{2}})$ Strouhal number deviation from the local neutral value. It is clear that A_∞ and Θ'_∞ satisfy the upstream boundary conditions (3.3) and (3.4) and that the mean-flow divergence effects are accounted for by the linear terms in λx_2. These effects eventually drive the growth rate to zero and then cause the instability wave to decay. The point of ultimate maximum amplitude is equal to the linear neutral stability point. It is important to realize, however, that this ultimate maximum amplitude may not be reached in an experiment since once the linear growth rate has been reduced owing to nonlinear effects other disturbances not accounted for in the present theory could then be faster growing and may become large enough to invalidate the theory.

As in II, the critical-layer vorticity equation correct to, but not including, $O(\epsilon)$ terms, can be written in the equilibrium form, i.e. $\mathscr{L}_e \Omega = 0$, by simply shifting the transverse coordinate y, here, by the amount

$$y_s = \epsilon^{\frac{1}{2}} \left\{ y_{1c} + \frac{1}{U_c'} \left[\frac{1}{\alpha_0} (U_c \Theta'_\infty + S_1) - c_{1N} \right] \right\}, \tag{3.28}$$

where
$$y_{1c} = \frac{c_{1N}}{U_c'} - 2\lambda x_2 c_1^{(0)}, \tag{3.29}$$

$$c_{1N} = \frac{\lambda x_2 U_c'}{U_c'''}\left(\frac{U_c' U_c'''}{U_c''^2} - \frac{U_c^{iv}}{U_c''}\right); \tag{3.30}$$

y_{1c} is the $O(\epsilon^{\frac{1}{2}})$ displacement of the mean-flow inflexion point and c_{1N} is the $O(\epsilon^{\frac{1}{2}})$ change in the local (linear) neutral phase velocity, both due to the slow streamwise divergence of the mean flow. Thus, analogous to II, the critical layer is shifted by the small amount $\epsilon^{\frac{1}{2}}(U_c \Theta_\infty' + S_1 - \alpha_0 c_{1N})/\alpha_0 U_c'$ from the actual basic-flow inflexion point, which is a small amount compared to its $O(\epsilon^{\frac{1}{3}})$ thickness.

4. The composite solution

The upstream linear unsteady flow can be determined by using weakly non-parallel stability theory (see Appendix D). The resulting solution, uniformly valid on the slow outer streamwise lengthscale $x_3 = O(1)$, can be taken as the real part of

$$\psi^{(o)} = A^{(o)}(x_3)\,\hat{\phi}_1^{(o)}(y; x_3) \exp\left\{i\left[\int_{x_e}^{x} \alpha(x_3)\,dx - St\right]\right\}, \tag{4.1}$$

where $\hat{\phi}_1^{(o)}$ denotes the spatially growing eigensolution to the Rayleigh stability problem using the streamwise mean-flow velocity at the location x_3, $\alpha = \alpha_r + i\alpha_i$ is the corresponding complex eigenvalue, $A^{(o)}$ is the slowly varying amplitude function (determined through a solvability condition in an appropriate multiple-scale perturbation expansion in powers of the slow mean-flow viscous divergence rate $1/R$), and x_e is the excitation (or a reference) position.

As the nonlinear region is approached (i.e. as $x_3 \to 0-$), $\hat{\phi}_1^{(o)} \to \hat{\phi}_1$ of §2, and it can be shown, either by inspection of the classical analysis of a perturbation about the neutral point (e.g. Yih 1969, p. 481) or, equivalently, by carrying out a growth critical-layer analysis, that

$$i\alpha \to i\alpha_0 - \tfrac{1}{2}\epsilon^{\frac{1}{2}} S_1 \sigma^{\dagger}, \tag{4.2}$$

where α_0 is the neutral wavenumber and $\sigma^{\dagger}$ is given by (2.25). The inner limit of the outer weakly non-parallel solution is, thus, given by

$$\psi^{(o)} \to \psi^{(o/i)} = A_0^{\dagger} \hat{\phi}_1(y) \exp\left(i\alpha_0 \zeta - \tfrac{1}{2}\int_0^{x_1} S_1 \sigma^{\dagger}\,dx_1\right), \tag{4.3}$$

where
$$A_0^{\dagger} = A^{(o)}(0) \exp\left[i \int_{x_e}^{0} \alpha(x_3)\,dx\right]. \tag{4.4}$$

The inner nonlinear solution $\psi^{(i)}$ is given by the second term on the right-hand side of (2.7) and it follows from (2.24) that $\psi^{(i)} \to \psi^{(o/i)}$ as $x_1 \to 0+$, i.e. that the solutions in the two different streamwise regions match. A uniformly valid composite solution can then be constructed by using the multiplicative rule (e.g. Van Dyke 1975)

$$\psi^{(c)} = \frac{\psi^{(o)}\psi^{(i)}}{\psi^{(o/i)}}, \tag{4.5}$$

which upon substituting the different solutions and using (2.25), (2.31), (2.34), (2.36), and (2.37) becomes

$$\psi^{(c)} = A(\bar{x}) \exp\left(-\int_0^{\bar{x}} \sigma\,d\bar{x}\right) A^{(o)}(x_3)\,\hat{\phi}_1^{(o)}(y; x_3) \exp\left\{i\left[\int_{x_e}^{x} \alpha(x_3)\,dx - St\right]\right\}, \tag{4.6}$$

where $A(\bar{x})\exp\left(-\int_0^{\bar{x}}\sigma\,\mathrm{d}\bar{x}\right)$ can be interpreted as a universal nonlinear correction factor, which depends only on $\bar{U},\bar{\lambda},\mu$, and the shifted coordinate $\bar{x}$. The latter coordinate is given in terms of the original coordinate x by the implicit relationship

$$\int_0^{\bar{x}}\sigma_r\,\mathrm{d}\bar{x}=\ln\left\{\frac{\alpha_0^2 U_c'\left|A^{(0)}(0)\exp\left[\mathrm{i}\int_{x_c}^{x}\alpha(x_3)\,\mathrm{d}x\right]\right|}{(-\frac{1}{2}\bar{U}S_1)^2}\right\}, \tag{4.7}$$

which is obtained by combining (2.25), (2.31), (2.36), and (4.2).

As $x_1\to+\infty$, the streamwise region where non-parallel effects again are important is approached. For $x_2=O(1)$, a (linear) growth critical-layer analysis shows that

$$\mathrm{i}\alpha\to\mathrm{i}\alpha_0+\epsilon^{\frac{1}{2}}(\mathrm{i}\alpha_1-\tfrac{1}{2}S_1^{(A)}\sigma^{\dagger}), \tag{4.8}$$

where α_1 is the $O(\epsilon^{\frac{1}{2}})$ change in the neutral wavenumber due to the slowly changing local conditions and $S_1^{(A)}$ is the actual $O(\epsilon^{\frac{1}{2}})$ Strouhal number deviation from the local neutral value; α_1 and $S_1^{(A)}$ are given by (3.26) and (3.27). Combination of (2.36), (4.4), (4.7), and (4.8) gives that

$$\int_{\bar{x}_0}^{\bar{x}}\sigma_r\,\mathrm{d}\bar{x}=-\tfrac{1}{2}\int_0^{x_1}\gamma S_1^{(A)}\sigma_r\,\mathrm{d}x_1, \tag{4.9}$$

from which it follows that

$$\bar{x}=-\tfrac{1}{2}\int_0^{x_1}\gamma S_1^{(A)}\,\mathrm{d}x_1+\bar{x}_0\approx-\frac{1}{2\epsilon^{\frac{1}{2}}}\int_0^{x_2}\gamma S_1^{(A)}\,\mathrm{d}x_2. \tag{4.10}$$

The first two members of (4.10) are simply the extension of (2.31) to the streamwise region $x_2=\epsilon^{\frac{1}{2}}x_1=O(1)$.

Furthermore, (2.36), (2.37), (4.10), (C 1), (C 2), (C 4), and (C 8)–(C 13) show that the universal nonlinear correction factor in (4.6)

$$A(\bar{x})\exp\left[-\int_0^{\bar{x}}\sigma\,\mathrm{d}\bar{x}\right]\to\frac{a_\infty}{A_0^{\dagger}}\left(\frac{U_c'}{\alpha_0^2}\right)^{\frac{1}{3}}$$
$$\times\left(-\tfrac{1}{2}\lambda\int_0^{x_1}\frac{\gamma S_1^{(A)}}{\chi^2}\mathrm{d}x_1\right)^{\frac{2}{3}}\exp\left[\tfrac{1}{2}\int_0^{x_1}\left(\sigma+\mathrm{i}\frac{\theta_\infty'-\chi\mu}{\chi^2}\right)\gamma S_1^{(A)}\,\mathrm{d}x_1-\mathrm{i}(\Theta_0-X_0')\right], \tag{4.11}$$

as $x_1\to+\infty$, with $x_2=\epsilon^{\frac{1}{2}}x_1=O(1)$, where X_0' is given by (C 10) and Θ_0 is a constant phase factor that can only be determined by going to a higher order in the large-$\bar{\lambda}\bar{x}$ asymptotic expansion (than was carried out in II) and then matching with the numerical solution for the non-equilibrium nonlinear critical-layer region. By now combining (4.4), (4.6), (4.8), and (4.11), it follows that

$$\psi^{(c)}\to a_\infty\left(\frac{U_c'}{\alpha_0^2}\right)^{\frac{1}{3}}\left(-\frac{\lambda}{2\epsilon^{\frac{1}{2}}}\int_0^{x_2}\frac{\gamma S_1^{(A)}}{\chi^2}dx_2\right)^{\frac{2}{3}}\hat{\phi}_1\exp\left\{\mathrm{i}\left[\alpha_0\zeta-\frac{1}{\epsilon^{\frac{1}{2}}}\left(\Theta_{\infty 0}+\int_0^{x_2}\Theta_\infty'\,\mathrm{d}x_2\right)\right]\right\}, \tag{4.12}$$

as $x_1\to+\infty$, with $x_2=\epsilon^{\frac{1}{2}}x_1=O(1)$, where $\Theta_{\infty 0}=\epsilon^{\frac{1}{2}}(\Theta_0-X_0')$, and Θ_∞' is given by (3.25). By comparing (4.12) with the assumption (3.2) and the results (3.24) and (3.25), it is clear that the region $x_2=O(1)$ is automatically contained in the composite solution (4.6), i.e. the latter is valid up to, and some distance beyond, the linear neutral point.

Equation (4.7) can be replaced by the following expression, which is of the same formal asymptotic order in the inner nonlinear region where the nonlinear correction factor differs from unity:

$$\int_0^{\bar{x}} \sigma_r \, \mathrm{d}\bar{x} \approx \ln\left\{\frac{\alpha_0^2 U_c' \left| A^{(0)}(x_3) \exp\left[\mathrm{i}\int_{x_e}^{x} \alpha(x_3)\,\mathrm{d}x\right]\right|}{(-\frac{1}{2}\bar{U}S_1)^2}\right\}, \tag{4.13}$$

where the parameters now also are allowed to vary with the slow streamwise coordinate x_3. The streamwise location of the inner nonlinear region is automatically set by the linear instability-wave growth when $\bar{x}$ is determined using (4.13). If the argument of the natural logarithm in (4.13), which can be interpreted as the ratio of the instability-wave amplitude and the square of a measure of the detuning from the local neutral conditions, remains much less than unity in the streamwise region of interest, then nonlinear effects are not important in that region.

The first step in obtaining a uniformly valid solution for the mean flow is to form an additive transverse composite solution in the inner flow region, $x_1 = O(1)$, where the nonlinear effects are important. Pertinent details about the mean-flow parts of the expansions outside and inside the critical layer, (2.5) and (2.17), are given in Appendices A and B. By then forming the streamwise composite solution from the solution valid on the x_3 scale and the transverse composite solution valid on the x_1 scale, the following uniformly valid (in both streamwise and transverse directions) results for the mean streamwise velocity and minus the mean vorticity are obtained:

$$U_M^{(c)} = U^{(0)}(y; x_3) + \tfrac{1}{2}\epsilon^{\frac{3}{2}} \int_{-\infty}^{Y} Q_0^{\dagger} \, \mathrm{d}Y + O(\epsilon^2 \ln \epsilon), \tag{4.14}$$

$$\Omega_M^{(c)} = \frac{\partial U^{(0)}(y; x_3)}{\partial y} + \tfrac{1}{2}\epsilon Q_0^{\dagger} + O(\epsilon^{\frac{3}{2}}), \tag{4.15}$$

where $U^{(0)}(y; x_3)$ is the mean-flow solution (computed in the absence of the instability wave) valid on the outer scale x_3 and $Q_0^{\dagger}$ is twice the period average of $Q^{\dagger}$. Outside the critical layer, the terms involving $Q_0^{\dagger}$ in (4.14) and (4.15) vanish and in addition the equations are correct to $O(\epsilon^2)$, the magnitude of the Reynolds stresses.

The maximum of the mean vorticity will occur inside the critical layer and it follows that the uniformly valid vorticity thickness is given by

$$\delta^{(c)} = \delta^{(0)}\left[1 + \epsilon \frac{U_c'''(-\frac{1}{2}\bar{U}S_1)^2 \bar{Q}_{\max}}{\alpha_0^2 U_c'^3 \bar{U}}\right], \tag{4.16}$$

where $\delta^{(0)}(x_3)$ is the vorticity thickness of the (streamwise) outer solution,

$$\bar{Q}_{\max} = \left[Q_0 - \tfrac{1}{2}\bar{U}\left(\eta - \frac{2}{\bar{U}}\right)^2\right]_{\max}, \tag{4.17}$$

and Q_0 is twice the period average of Q.

5. Results and discussion

The asymptotic theory of the previous sections accounts for the instability-wave nonlinearity as well as the viscous spreading of the basic flow. The main purpose of this section is now to test the resulting uniformly valid composite solution by a comparison with suitable experiments. Among the requirements for the experiments

are that the shear layer initially is laminar and, in particular, that sufficient details are available about the early development of both the instability wave and the mean flow so that a first-principle comparison can be assured. In this respect, it is necessary that there is an initial streamwise region where the flow can be treated as a superposition of a linear instability wave and an undisturbed mean flow. An excellent discussion of relevant experimental literature, as well as other topics of interest, can be found in the review paper by Ho & Huerre (1984). Comparisons will be made here with experimental data for plane-jet shear layer (Thomas & Chu 1989), a circular-jet shear layer (Freymuth 1966), and a mixing layer behind a splitter plate (C.-M. Ho & Y. Zohar 1989, private communication).

The following procedure or strategy was used to ensure a first-principle comparison between theory and experiment. First, the mean streamwise velocity profile was fitted by an analytical expression at (only) one streamwise measuring station – located sufficiently far upstream to ensure that the instability wave had a small enough amplitude that the local mean flow was unaffected by its presence. Since it is impossible to establish how small is small enough on an *a priori* basis, the superposition assumption was tested as part of the computations. Second, the downstream evolution of the undisturbed mean flow was computed using a 'boundary-layer' type numerical code with the fitted profile used as initial condition. The computed mean flow was then compared to the measured one to partially verify that the mean-flow initially was unaffected by the instability wave (a full verification would also involve a demonstration that the instability wave initially grows according to linear theory). Third, the Rayleigh stability problem was solved numerically using the computed local velocity profiles. The weakly non-parallel corrections [in this case also including viscous-dissipation effects which enter at the same order as the non-parallel ones (Lanchon & Eckhaus 1964), see Appendix D] were computed and the overall results were integrated in the streamwise direction to predict the amplitude evolution of the linear instability wave. At this point, the linear growth of the initial instability wave could also be verified. It is also worth noting that a first-principle comparison would not be achieved if measured profiles were used instead of the computed (undisturbed) ones since the mean flow is affected by the instability wave in the roll-up region.

Fourth, the parameters $\bar{U}$, $\bar{\lambda}$, and μ and the equivalent nonlinear coordinate $\bar{x}$, cf. (2.30), (2.38), (2.28), and (4.13), were evaluated as functions of the streamwise location from these results and the streamwise energy of the instability wave at the initial measuring station. Because of the slowly varying mean flow, this step, in fact, also involves the determination of the local linear neutral conditions as functions of the streamwise location. Since $\bar{U}$, $\bar{\lambda}$, and μ depend on the streamwise location, these parameters are then known as weak functions of $\bar{x}$. Finally, the nonlinear correction factor in (4.6) was evaluated by solving the nonlinear non-equilibrium critical-layer problem (2.39)–(2.42) with slowly varying parameters. The details of the weakly non-parallel linear stability problem and some remarks about the mean-flow computation are given in Appendix D. The numerical treatment of the nonlinear non-equilibrium critical-layer problem is similar to II, but the parameters now are evaluated locally.

The Thomas & Chu (1989) experiment involves a plane jet issuing from a two-dimensional nozzle ending in a slot of width $D = 12.7$ mm and height $H = 457$ mm. Although the mean-flow configuration is that of a submerged plane jet, the initial shear layers are completely non-interacting for the streamwise region of interest here (at most 1.5 slot-widths downstream of the plane-jet orifice) and can therefore be treated independently. The reader is referred to Thomas & Chu's (1989) paper for

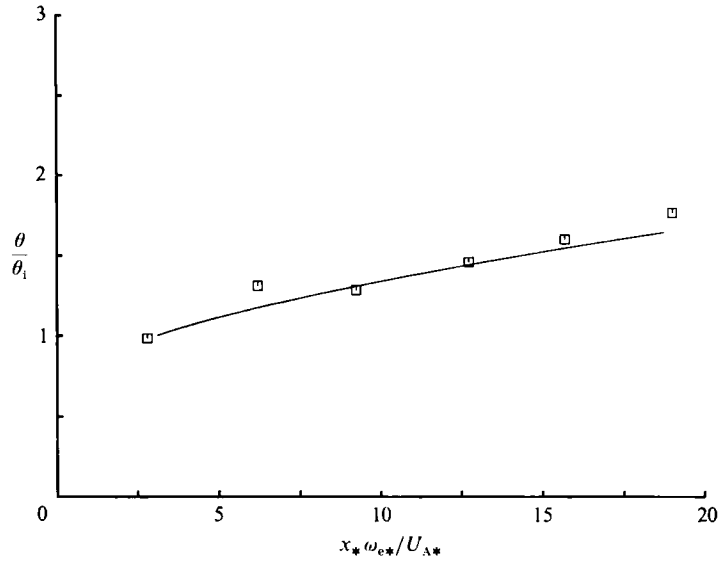

FIGURE 2. Comparison of computed undisturbed-flow momentum thickness (——) with data from Thomas & Chu's (1989) plane-jet shear-layer experiment (□).

complete details about their experiment. They used a relatively low-level single-frequency acoustic excitation of frequency $\omega_{e*}/2\pi = 750$ Hz to somewhat organize the disturbance flow and to provide a phase reference. The average velocity of the streams $U_{A*} = 4.8$ m s^{-1} (half the exit velocity), and the kinematic viscosity of the air is computed be $\nu = 14.7 \times 10^{-6}$ m s^{-2} from the stated slot-width exit-velocity Reynolds number of 8300. This leads to a convective lengthscale $L_\omega = U_{A*}/\omega_{e*} = 1.02$ mm and a frequency parameter $F = \nu\omega_{e*}/U_{A*}^2 = 3.01 \times 10^{-3}$. The Strouhal number (based on the average stream velocity and half the local vorticity thickness) is estimated here to be 0.304 at their first mean-flow measuring station, located 0.25 slot-widths downstream of the plane-jet orifice. The aforementioned condition on the instability-wave amplitude was judged to be satisfied at this measuring station and, using a least-squares procedure, a good fit of the experimental mean-flow profile (Thomas & Chu 1989, figure 2) could be obtained with an analytical expression of the form

$$U(y) = 1 + Ra\, F(Cy), \tag{5.1}$$

$$F(u) = \tanh u + (A - B \tanh u)\,\mathrm{sech}^2(\tfrac{1}{3}u), \tag{5.2}$$

where $Ra = (U_1 - U_2)/(U_1 + U_2)$ (= 1, here) is commonly called the velocity ratio of the shear layer, and A, B, and C are constants.

Both a shear-layer code (where two free-stream conditions are imposed) and a plane-jet code (where one of the free stream-conditions is replaced by a centreline symmetry condition) were then used to determine the mean-flow evolution. It was concluded from the plane-jet results as well as from a comparison with the results of the (isolated) shear-layer code that there was no detectable interaction between the two shear layers in the streamwise region of interest. The isolated-shear-layer assumption is therefore completely adequate for the present computations.

The computed streamwise evolution of the undisturbed-flow momentum thickness is compared with the experimental data (Thomas & Chu 1989, figure 3) in figure 2. The agreement is good even in the streamwise region where nonlinear effects are

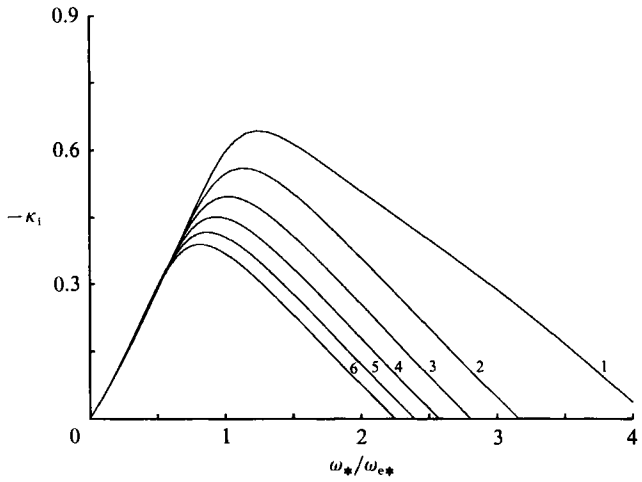

FIGURE 3. Computed linear parallel-flow spatial growth rates for the mean-flow measurement stations in Thomas & Chu's (1989) plane-jet shear-layer experiment.

expected to be important for the disturbance flow (roughly the second half of the displayed streamwise region). This is because the nonlinear momentum-thickness correction is $O(\epsilon^2)$ and therefore can be quite small. Furthermore, the agreement can actually be considered to be quite good if one takes into account that the relative error in the measurements is likely to be large because of the small values of the momentum thickness in the streamwise region shown in this figure.

Figure 3 shows curves of the linear parallel-flow spatial growth rate corresponding to the mean-flow measuring stations $x_* = \frac{1}{4}nD$, $n = 1, 2, \ldots, 6$, in the Thomas & Chu (1989) experiment. The calculations were based on velocity profiles from the undisturbed mean-flow computation, and the abscissa and ordinate have been normalized using the angular frequency of the forcing and the convective lengthscale $L_\omega (= U_{A*}/\omega_{e*})$, respectively. These growth-rate curves are, apart from the first, nearly self-similar in the sense that they nearly can be collapsed onto a single curve when local scales based on the shear-layer vorticity thickness are used in the normalization. However, the present global scaling is used to illustrate how the quasi-parallel linear growth rate changes as the forced disturbance ($\omega_*/\omega_{e*} = 1$) propagates downstream. Note that the non-dimensional frequency of unity is less than the peak frequency of the local growth rate curve at the first streamwise station. The overall magnitude of the growth rate then decreases and the peak of the local growth-rate curve moves towards smaller values of ω_*/ω_{e*} with increasing downstream distance. The quasi-parallel linear growth rate of the forced disturbance is therefore monotonically decreasing with downstream distance. As indicated below, the nonlinear effects first come into play at the streamwise position where ω_{e*} is just larger than the peak frequency of the corresponding local growth-rate curve. Note that, at least from a theoretical point of view, the linear growth rate has become small at this point. In fact $\epsilon^{\frac{1}{3}}$ would be about 0.26–0.32 for an disturbance amplitude of about 7–10% of the characteristic mean-flow velocity, which is typical of the Thomas & Chu (1989, figure 11) experiment, so that the linear growth rate in the aforementioned region is consistent with the inherent scaling assumptions in the present analysis, cf. (2.2) and (2.4). It is also important to note that the linear growth-rate curves corresponding to this particular experiment are quite straight from the maximum growth rate to the neutral point, which indicates that the linear

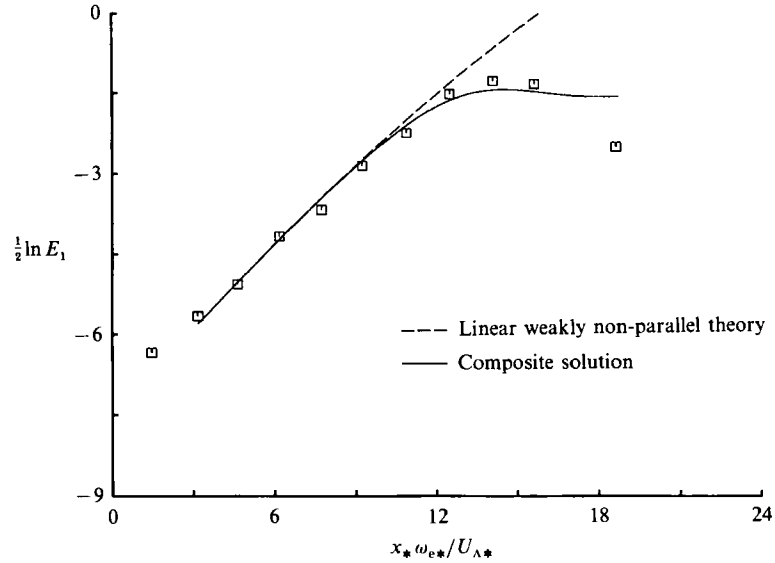

FIGURE 4. Comparison of composite solution accounting for both nonlinear critical-layer effects and viscous mean-flow spreading with instability-wave energy data from Thomas & Chu's (1989) plane-jet shear-layer experiment.

perturbation about the local neutral point will provide a good representation of the actual quasi-parallel linear growth rate almost all the way up to the peak value. This suggests that the near-neutral assumption of the present theory will provide a good approximation in the flow region of interest. These considerations, along with the fact that asymptotic analysis is a rational way to account for the essential physics of the problem, leads one to expect that the nonlinear non-equilibrium critical layer theory will provide a good description of the flow even though the nonlinear effects, in a sense, have to come in quite early.

An appropriate measure of the spatially evolving instability-wave amplitude in a non-parallel flow is given by the energy associated with the streamwise velocity component u_* of the instability wave,

$$E_1 = \frac{1}{2L_\omega U_{\Lambda*}^2}\int_{-\infty}^{+\infty} \overline{u_*^2}\,\mathrm{d}y_* = \tfrac{1}{2}S\int_{-\infty}^{+\infty}\overline{\left[Re\left(\frac{\partial\psi^{(c)}}{\partial y}\right)\right]^2}\,\mathrm{d}y, \tag{5.3}$$

where the overbar denotes a period average and $\psi^{(c)}$ is given by (4.6).

The experimental instability-wave energy was obtained from Thomas & Chu's (1989) figure 11, which was derived from cross-stream integrated shear-layer power spectra normalized by the initial jet half-width $\approx \frac{1}{2}D$ (the normalization information was inadvertently omitted from their paper). The initial energy input to the nonlinear calculation was then determined by optimizing the fit of the linear weakly non-parallel solution with the first few data points rather than using the experimental value at the first (mean-flow) measuring station; it was taken to be $E_{1i} = 9\times10^{-6}$. This procedure was used in order to minimize the influence on the overall results of the unavoidable error in the measurements at any given station.

Figure 4 shows the excellent agreement between the composite solution and the experimental results. (No experimental mean-flow data are available until the second instability-wave data point – this is why the comparison starts at the corresponding

streamwise location.) While the theory does not predict the last data point very well, Thomas & Chu's (1989) figure 11 shows the flow to be dominated by subharmonics of the sum and difference frequencies of the forcing frequency (750 Hz) and the so-called jet-column frequency of 125 Hz at that streamwise station and hence that the assumptions of the theory are probably violated there. Note that one of the inherent assumptions of the theory is that the disturbance flow is dominated by the forcing frequency outside the critical layer. However, all harmonics are generated and are on equal footing inside the critical layer since the flow is strongly nonlinear there. The less drastic amplitude reduction predicted by the composite solution once the peak value is passed is also reminiscent of the experimental results obtained by Freymuth (1966), see below. Figure 4 also shows that there is an initial streamwise region where the disturbance is well described by weakly non-parallel linear theory based on undisturbed mean-flow profiles which, as pointed out above, is an essential part of assuring that a first-principle comparison is being carried out. As pointed out by Thomas & Chu (1989) and as can be seen clearly from the present figures 3 and 4, the nonlinear instability wave saturates well upstream of the linear neutral stability point for the undisturbed mean flow. The saturation level therefore is not related to the ultimate maximum amplitude of §3 for the reason pointed out in that section. The effective saturation in the composite solution is associated with the first of the local amplitude maxima caused by oscillations in the growth rate, see I and II. The predicted instability-wave evolution and saturation is in excellent agreement with the experiment in the streamwise region where the experimental disturbance flow is dominated by the forced frequency, i.e. within the expected range of validity of the theory.

A comparison will also be carried out here with the only case in Freymuth's (1966) investigation of the initial shear-layer transition process for which the mean-flow velocity distribution at the beginning of the linear region was documented. This case, described in his figures 4–10 and 29 and the accompanying discussion, was a circular jet with a nozzle diameter of 75 mm, a jet-core velocity of 8 m s^{-1}, which was acoustically excited at 416 Hz. The value of the kinematic viscosity consistent with the information given is 14.8×10^{-6} m^2 s^{-1}. This leads to a convective lengthscale $L = 1.53$ mm and a frequency parameter $F = 2.42 \times 10^{-3}$. The mean velocity distribution at the initial or reference station, located about ten local momentum thicknesses downstream of the nozzle lip, was found by Freymuth (1966) to be quite well described by a hyperbolic-tangent velocity profile, i.e. (5.1), (5.2) with $Ra = 1$ and $A = B = 0$. Thus, the Strouhal number at the reference station was 0.300 when using the present normalization. Drubka (1981, figure 18) also found in his circular-jet shear-layer investigation that the mean flow was well described by a hyperbolic-tangent profile close to the jet nozzle with the mean velocity then developing towards a self-similar profile in the linear region.

The streamwise evolution of the mean flow was determined using the shear-layer code with a hyperbolic-tangent velocity profile as upstream condition. Unfortunately, figure 4 in Freymuth (1966) only shows the momentum-thickness evolution for a rather limited streamwise distance and all data points except one are clustered in the vicinity of the reference station. The computed momentum thickness, of course, fits the data in the figure quite well for the clustered points, but the somewhat isolated last point in that figure has a value about 11 % lower than the computed value. Little weight should be placed on this discrepancy, however, in view of the inherent difficulty in measuring the momentum thickness 'due to hot-wire rectification errors in the zero-velocity free stream'. Drubka (1981) also reported a

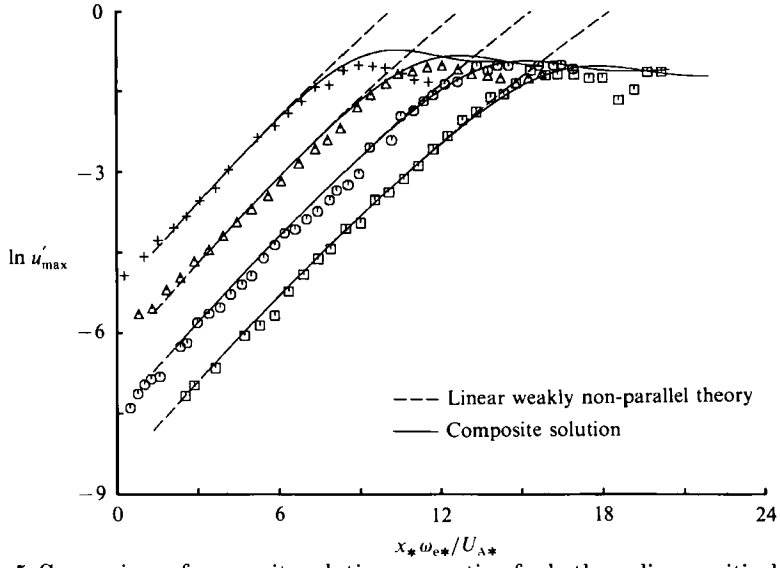

FIGURE 5. Comparison of composite solution accounting for both nonlinear critical-layer effects and viscous mean-flow spreading with instability-wave amplitude data for four excitation levels from Freymuth's (1966) circular-jet shear-layer experiment.

momentum-thickness evolution in his experiment that was contrary to Freymuth's (1966) observation but which is in line with the computed values here.

Freymuth used the transverse maximum of the r.m.s. value of the streamwise velocity component of the instability wave as a measure of the disturbance amplitude, i.e. $u'_{max} = \max_y u'$, where

$$u'^2 = \frac{\overline{u_*^2}}{U_{A*}^2} = \overline{\left(\frac{\partial \psi^{(c)}}{\partial y}\right)^2} \tag{5.4}$$

and $\psi^{(c)}$ is given by (4.6). Figure 5 shows a comparison of the composite solution with Freymuth's (1966, figure 10) amplitude-evolution data for four different excitation levels. The values of $\max_y u'$ at the reference station corresponding to the four curves are 4×10^{-4}, 1.2×10^{-3}, 3.6×10^{-3}, and 1.1×10^{-2}, respectively. This figure confirms that there is an initial streamwise region where the disturbance is well described by weakly non-parallel linear stability theory based on the undisturbed mean flow and that, of course, this region becomes shorter with increasing initial amplitude. The composite solution is in good agreement with the experimental data corresponding to the lowest excitation level, except for what appears to be a local minimum in the experimental data just past the first nonlinear saturation. This discrepancy could be caused by an interaction with naturally occurring 'subharmonic' disturbances that are not accounted for in the present theory, as in the comparison above with the Thomas & Chu (1989) experiment, but unfortunately Freymuth (1966) does not provide any information about such disturbances. The agreement between theory and experiment is very good at the next higher level of initial amplitude, however. This gives some further circumstantial evidence for the conjecture above since the naturally occurring 'subharmonic' disturbances probably have not reached a sufficient amplitude to ultimately influence the fundamental disturbance in any but the least excited case where the saturation occurs the furthest downstream. For the highest two excitation levels, the nonlinear effects come into play upstream of the

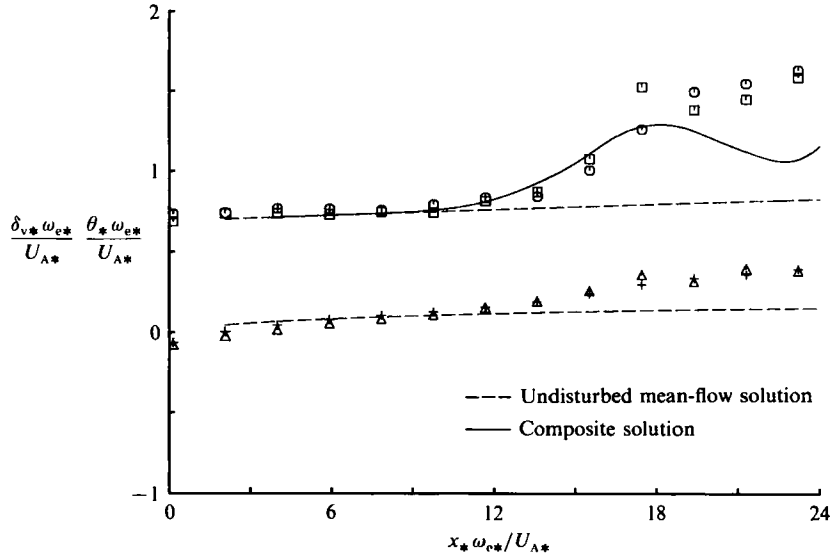

FIGURE 6. Comparison with vorticity-thickness and momentum-thickness data from C.-M. Ho & Y. Zohar's (unpublished) mixing-layer experiment: ⊡, vorticity thickness, low-level forcing at natural frequency; ⊙, vorticity thickness, unforced case; △, momentum thickness, low-level forcing at natural frequency; +, momentum thickness, unforced case.

streamwise location (here about $9L_\omega$) where ω_{e*} corresponds to the peak in the local linear growth-rate curve. Since the relative importance of the linear effects are then overestimated in the nonlinear theory, the composite solution, as can be seen in figure 5, will increasingly underestimate the deviation from the weakly non-parallel linear theory with increasing excitation level. The composite solution yields a qualitatively correct result for the highest two levels of excitation here, however.

The third experiment used for comparison consists of unpublished data kindly supplied by C.-M. Ho & Y. Zohar (1989) of the Department of Aerospace Engineering, University of Southern California, for a mixing layer behind a splitter plate. A relatively low-level forcing at the so-called natural shear-layer frequency (here 355 Hz) was used to excite the shear layer, but data were also supplied for the corresponding unforced case. The average velocity and the velocity ratio of the two streams were 7.5 m s^{-1} and $Ra = 0.652$, respectively. The shear-layer facility is the same as used in Huang & Ho (1990) and further information about the wind tunnel can be found in that paper. The convective lengthscale is $L_\omega = 3.33$ mm and, with $\nu = 15 \times 10^{-6}$ m^2 s^{-1}, the frequency parameter becomes $F = 6.03 \times 10^{-4}$ for this experiment. In order to avoid trailing-edge effects, the streamwise reference station was here taken to be the second streamwise measuring station, located 6.9 mm downstream of the trailing edge of the splitter plate (the corresponding distance for the first station is 0.5 mm), and the local Strouhal number was estimated to be 0.350. The velocity profile, which still has a sizable wake defect at this station, was fitted with (5.1), (5.2) and the downstream evolution of the mean flow was determined using the shear-layer code. The initial instability-wave energy was taken to be $E_{1i} = 1.6 \times 10^{-7}$ for the nonlinear stability computation.

Figure 6 shows the shear-layer vorticity thickness, including the additional thickening produced by the nonlinear instability wave, the momentum thickness, and the corresponding experimental data as functions of the streamwise distance, and figure 7 shows a comparison of the experimental data for the streamwise

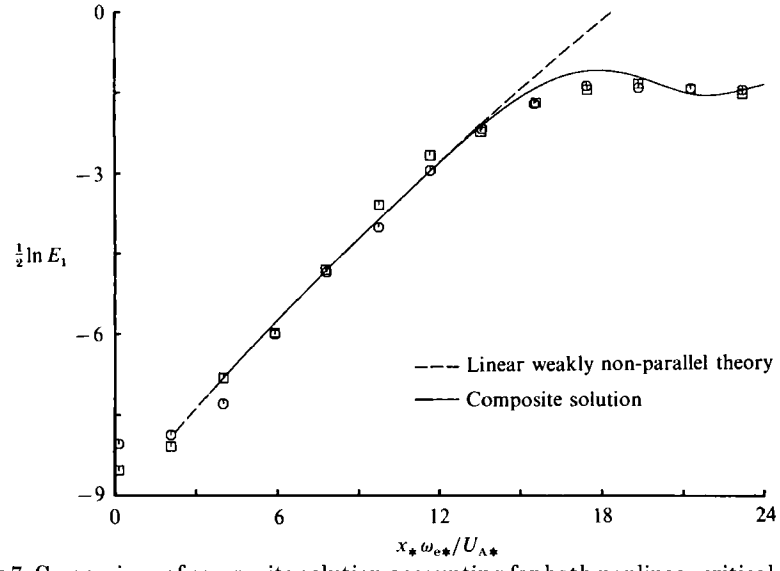

FIGURE 7. Comparison of composite solution accounting for both nonlinear critical-layer effects and viscous mean-flow spreading with instability-wave energy data from Ho & Zohar's mixing-layer experiment: ⊡, low-level forcing at natural frequency; ⊙, unforced case.

evolution of the instability-wave energy and the composite solution, cf. (5.3). These figures show that there is an initial streamwise region where the mean flow and the instability wave are well described by the undisturbed mean-flow computation and weakly non-parallel linear stability theory based on that computation, respectively. The agreement between the composite instability-wave energy and the experimental data is good in this case also. The initial additional thickening is well described by the composite vorticity, but the later oscillation in the composite solution is not reflected in the experimental data. The main effects of the wake component on the local linear stability properties are an increase in the maximum value of the growth rate and a reduction in the unstable frequency range. However, the lower value of the frequency parameter compared to the experiments discussed above means, as can be seen in figure 6, that the undisturbed shear layer spreads less over the streamwise region of interest in this case. Consequently, the local Strouhal number of the instability wave, initially being just slightly less than that corresponding to the maximum growth rate, remains close to the peak value at all streamwise stations. This, as noted above, leads to an overestimation of the relative importance of linear effects in the nonlinear theory and, hence, is the most likely cause for the small overshoot in the composite instability-wave energy and probably also for the oscillation in the composite vorticity thickness.

The present investigation has shown that the nonlinear instability wave behaviour is determined mainly in a small transverse region located at the position where the mean-flow vorticity is at maximum and that the vorticity thickness is a sensitive measure of the nonlinear disturbance effects on the mean flow. One can but hope that this (local) measure of the shear layer thickness, rather than the more traditional and global measure, the momentum thickness, will be documented in future experimental investigations. The vorticity thickness is, arguably, the more fundamental of the two since the momentum thickness has no precise physical interpretation for the doubly unbounded flows considered herein. (As can be seen in figure 7, the momentum thickness can also take on a negative value for shear-layer flows with a sufficient

wake component.) The vorticity thickness is also the appropriate measure to be used in order to collapse linear stability calculations for different shear-layer profiles (Monkewitz & Huerre 1982).

The author wishes to thank Drs C.-M. Ho and Y. Zohar for providing the mixing-layer data.

Appendix A. The main part of the shear layer

The first term, ψ_0, in the main-shear-layer expansion (2.5) is related to the zeroth-order term in the (local) basic-flow Taylor series expansion and, hence, is determined by the upstream history of the basic flow. For small values of y, ψ_0 can be expressed as

$$\psi_0 = U_c y + \tfrac{1}{2}U_c' y^2 + \tfrac{1}{24}U_c''' y^4 + O(y^5), \tag{A 1}$$

where the subscript c denotes the value at the inflexion point of the basic flow. The other terms in (2.5) can be determined by an analysis valid on the streamwise scale x_1, however, and the next few $\psi_{n/2}(n>1)$ are governed by

$$\mathscr{L}_0\psi_1 = 0, \tag{A 2}$$

$$\mathscr{L}_0\psi_{\frac{3}{2}} = -\mathscr{L}_1\psi_1 + \lambda U''', \tag{A 3}$$

$$\mathscr{L}_0\psi_2 = -\mathscr{L}_1\psi_{\frac{3}{2}} - \Gamma_2 - \frac{\partial(\nabla^2\psi_1, \psi_1)}{\partial(\zeta, y)}, \tag{A 4}$$

$$\begin{aligned}\mathscr{L}_0\psi_{\frac{5}{2}} = -\mathscr{L}_1\psi_2 - \Gamma_{\frac{5}{2}} &- \frac{\partial(\nabla^2\psi_1, \psi_{\frac{3}{2}})}{\partial(\zeta, y)} \\ &- \frac{\partial(\nabla^2\psi_{\frac{3}{2}} + 2\partial^2\psi_1/\partial\zeta\,\partial x_1, \psi_1)}{\partial(\zeta, y)} - \frac{\partial(\nabla^2\psi_1, \psi_1)}{\partial(x_1, y)} + \lambda\nabla^4\psi_1,\end{aligned} \tag{A 5}$$

where

$$\mathscr{L}_0 = [(U-U_c)\nabla^2 - U'']\frac{\partial}{\partial\zeta}, \tag{A 6}$$

$$\mathscr{L}_1 = \left(-\frac{S_1}{\alpha_0}\frac{\partial}{\partial\zeta} + U\frac{\partial}{\partial x_1}\right)\nabla^2 + \left[2(U-U_c)\frac{\partial^2}{\partial\zeta^2} - U''\right]\frac{\partial}{\partial x_1}, \tag{A 7}$$

$$\Gamma_2 = \left[(3U-U_c)\frac{\partial}{\partial x_1} - 2\frac{S_1}{\alpha_0}\frac{\partial}{\partial\zeta}\right]\frac{\partial^2\psi_1}{\partial\zeta\,\partial x_1}, \tag{A 8}$$

$$\Gamma_{\frac{5}{2}} = \left[(3U-U_c)\frac{\partial}{\partial x_1} - 2\frac{S_1}{\alpha_0}\frac{\partial}{\partial\zeta}\right]\frac{\partial^2\psi_{\frac{3}{2}}}{\partial\zeta\,\partial x_1} + \left(U\frac{\partial}{\partial x_1} - \frac{S_1}{\alpha_0}\frac{\partial}{\partial\zeta}\right)\frac{\partial^2\psi_1}{\partial x_1^2}, \tag{A 9}$$

and ∇^2 denotes the Laplacian with respect to ζ and y.

As in II, substitution of (2.7) into (A 2) leads to (2.9) for $\hat{\phi}_1$ and the ζ-independent part of the $O(\epsilon^{\frac{3}{2}})$ problem (A 3) gives that

$$G(y) = U\left(\tfrac{1}{2}\int_0^y \frac{U''}{U^2}\,dy + c_1^{(0)}\right) = c_1^{(0)}U_c + c_1^{(0)}U_c' y + \frac{U_c'''}{4U_c}y^2 + O(y^3), \tag{A 10}$$

with the constant $c_1^{(0)}$, which simply corresponds to a transverse shift of the streamlines, determined by the global mean-flow variation. Substitution of the

$n = 3$ term of (2.8) into (A 3) produces (2.10) for $\Phi_{\frac{3}{2}}^{(m)}$, $m \geqslant 1$, and the ζ-independent part of the $O(\epsilon^2)$ and $O(\epsilon^{\frac{5}{2}})$ problems (A 4) and (A 5), gives that

$$\Phi_{\frac{3}{2}}^{(0)} = a_{\frac{3}{2}}^{(0)} U/U_c = a_{\frac{3}{2}}^{(0)}\left[1+\frac{U_c'}{U_c}y+O(y^3)\right], \tag{A 11}$$

$$\begin{aligned}\Phi_2^{(0)} = {}& \tfrac{1}{4}|A^+|^2 U\left\{\int_{\pm\infty}^{y}\frac{U''\hat{\phi}_1^2}{U(U-U_c)^2}\,\mathrm{d}y-\int_0^y[(\mathrm{D}\hat{\phi}_1)^2-\alpha_0^2\hat{\phi}_1^2]\right\}+\lambda^2 x_1^2 U\int_{\pm\infty}^{y}\frac{G'''}{U^2}\,\mathrm{d}y\\ &-P_{2\infty}^{\pm}U\int_0^y\frac{\mathrm{d}y}{U^2}+a_2^{(0)}U/U_c = \tfrac{1}{4}|A^+|^2\left\{\frac{U_c'''}{U_c'^2}\left(1+\frac{U_c'}{U_c}y\right)\ln\left|\frac{y}{2}\right|\right.\\ &\left.+U_c\int_{\pm\infty}^{0}\left[\frac{U''\hat{\phi}_1^2}{U(U-U_c)^2}-\frac{U_c'''}{U_c U_c'^2\sinh y}\right]\mathrm{d}y\right\}\\ &+\lambda^2 x_1^2 U_c\int_{\pm\infty}^{0}\frac{G'''}{U^2}\,\mathrm{d}y+a_2^{(0)\pm}+O(y),\end{aligned} \tag{A 12}$$

where $P_{2\infty}^{\pm}$ denotes the $O(\epsilon^2)$ mean-flow pressure at the edges of the shear layer, i.e. as $y\to\pm\infty$. It also follows from the first two members of (A 12) that the $O(\epsilon^2)$ jump in the streamwise mean velocity across the critical layer is given by

$$\Delta U_2 = \frac{U_c'}{U_c}(a_2^{(0)+}-a_2^{(0)-})-\tfrac{1}{4}|A^+|^2 U_c' J_3-\lambda^2 x_1^2 U_c' J_4-\frac{1}{U_c}(P_{2\infty}^{+}-P_{2\infty}^{-}), \tag{A 13}$$

where

$$J_3 = \int_{-\infty}^{+\infty}\frac{U''\hat{\phi}_1^2}{U(U-U_c)^2}\,\mathrm{d}y, \quad J_4 = \int_{-\infty}^{+\infty}\frac{G'''}{U^2}\,\mathrm{d}y. \tag{A 14, 15}$$

Equation (A 11) implies that there are non-vanishing $O(\epsilon^2)$ transverse mean-flow velocity components at the edges of the shear layer, i.e. as $y\to\pm\infty$. This necessitates an outer potential flow on the x_1 and $y_1 = \epsilon^{\frac{1}{2}}y$ scales. The requirement that the tangential velocity of these potential flows (one on each side of the shear layer) match the $O(\epsilon^2)$ streamwise mean flow velocities obtainable from (A 2) in the limit of $y\to\pm\infty$ yields the following pressure-displacement conditions:

$$P_{2\infty}^{\pm} = \mp\frac{U_\infty^{\pm 2}}{\pi U_c}\int_{-\infty}^{+\infty}\frac{a_{\frac{3}{2}}^{(0)\prime}(\tilde{x}_1)}{\tilde{x}_1-x_1}\,\mathrm{d}\tilde{x}_1, \tag{A 16}$$

where $U_\infty^{\pm}$ denotes the limit of U as $y\to\pm\infty$. However, as shown in Appendix B, $P_{2\infty}^{+} = P_{2\infty}^{-}$, and it then follows from (A 16) that, as in I,

$$a_{\frac{3}{2}}^{(0)} = P_{2\infty}^{+} = P_{2\infty}^{-} = 0. \tag{A 17}$$

Finally, a small-y analysis of the $O(\epsilon^2)$ problem (A 4) for $m > 0$ shows that

$$\begin{aligned}\Phi_2^{(m)} = {}& \delta_{m1}\frac{U_c'''}{\alpha_0^2 U_c'^3}\left(U_c\frac{\mathrm{d}}{\mathrm{d}x_1}-\mathrm{i}S_1\right)^2 A^+\ln|y|+a_2^{(m)}\\ &+\mathrm{Re}\left(\sum_{m=1}^{+\infty}C_2^{(m)}\mathrm{e}^{\mathrm{i}m\alpha_0\zeta}\right)y\ln|y|+O(y),\end{aligned} \tag{A 18}$$

where

$$\begin{aligned}C_2^{(m)} = {}& \frac{\mathrm{i}}{m\alpha_0 U_c'}\left(U_c\frac{\mathrm{d}}{\mathrm{d}x_1}-\mathrm{i}mS_1\right)\left[\left(\frac{U_c'''}{U_c'}+2\mathrm{i}\,m\alpha_0\frac{\mathrm{d}}{\mathrm{d}x_1}\right)a_{\frac{3}{2}}^{(m)}-2\mathrm{i}\,\alpha_0\delta_{m1}\frac{\mathrm{d}A^+}{\mathrm{d}x_1}\right]\\ &-\delta_{m2}\frac{A^{+2}}{8U_c'^2}(2b_1 U_c'''+\tfrac{1}{2}U_c^{\mathrm{iv}}).\end{aligned} \tag{A 19}$$

Appendix B. The critical-layer expansion

The first few terms in the critical-layer expansion (2.18), Ψ_0 to Ψ_{1L}, simply correspond to terms in the inner limit of the outer solution and are given by

$$\Psi_0 = \tfrac{1}{2}U_c' Y^2 + 2\lambda x_1 U_c c_1^{(0)} + \mathrm{Re}\,(A^\dagger \mathrm{e}^{\mathrm{i}\alpha_0\zeta}), \tag{B 1}$$

$$\Psi_{\frac{1}{2}} = 2\lambda x_1 c_1^{(0)} U_c' Y + \mathrm{Re}\left(\sum_{m=0}^{+\infty} a_{\frac{1}{2}}^{(m)} \mathrm{e}^{\mathrm{i}m\alpha_0\zeta}\right), \tag{B 2}$$

$$\Psi_{1L} = \frac{U_c'''}{8U_c'^2}|A^\dagger|^2 + \mathrm{Re}\left[\frac{U_c'''}{\alpha_0^2 U_c'^2}\left(U_c\frac{\mathrm{d}}{\mathrm{d}x_1} - \mathrm{i}S_1\right)\left(U_c\frac{\mathrm{d}}{\mathrm{d}x_1} - \mathrm{i}S_1 + \mathrm{i}\alpha_0 U_c' Y\right)A^\dagger \mathrm{e}^{\mathrm{i}\alpha_0\zeta}\right]; \tag{B 3}$$

Ψ_1 is the first non-trivial term in the critical-layer expansion (2.18) and is determined by the viscous critical-layer vorticity equations (2.19) and (2.20).

Of the next two terms in (2.18),

$$\Psi_{\frac{3}{2}L} = \frac{U_c'''}{8U_c U_c'}|A^\dagger|^2 Y + \tfrac{1}{2}\mathrm{Re}\left(\sum_{m=1}^{+\infty} C_2^{(m)} \mathrm{e}^{\mathrm{i}m\alpha_0\zeta}\right)Y, \tag{B 4}$$

where $C_2^{(m)}$ is given by (A 19), again simply corresponds to a term in the inner expansion of the outer solution, but $\Psi_{\frac{3}{2}}$ is non-trivial and is determined by

$$\mathscr{L}_{\mathrm{v}}\Omega_{\frac{3}{2}} = -U_c' Y\frac{\partial\Omega_1}{\partial x_1}, \tag{B 5}$$

$$\begin{aligned}\Omega_{\frac{3}{2}} \to {} & \tfrac{1}{6}U_c^{\mathrm{iv}} Y^3 + 2\lambda x_1\left[c_1^{(0)} U_c''' + \frac{1}{2}\left(\frac{U_c^{\mathrm{iv}}}{U_c} - \frac{U_c''' U_c'}{U_c^2}\right)\right]Y \\ & + \left[\frac{U_c^{\mathrm{iv}}}{2U_c'} + b_1\left(\alpha_0^2 + \frac{U_c'''}{U_c'}\right)\right]\mathrm{Re}\,[A^\dagger \mathrm{e}^{\mathrm{i}\alpha_0\zeta}] + \frac{U_c'''}{U_c'}\mathrm{Re}\left[\sum_{m=1}^{+\infty} a_{\frac{3}{2}}^{(m)} \mathrm{e}^{\mathrm{i}m\alpha_0\zeta}\right. \\ & \left. + \frac{\mathrm{i}}{\alpha_0 U_c'}\left(U_c\frac{\mathrm{d}}{\mathrm{d}x_1} - \mathrm{i}S_1\right)\left(\frac{U_c^{\mathrm{iv}}}{2U_c'''} + b_1\right)A^\dagger \mathrm{e}^{\mathrm{i}\alpha_0\zeta}\right] \quad \text{as} \quad Y \to \pm\infty,\end{aligned} \tag{B 6}$$

where $\mathscr{L}_{\mathrm{v}}$ is the viscous critical-layer operator in (2.19) and

$$\Omega_{\frac{3}{2}} = \frac{\partial^2 \Psi_{\frac{3}{2}}}{\partial Y^2} + \mathrm{Re}\left[2\mathrm{i}\alpha_0\frac{\mathrm{d}A^\dagger}{\mathrm{d}x_1}\mathrm{e}^{\mathrm{i}\alpha_0\zeta} - \sum_{m=1}^{+\infty} a_{\frac{3}{2}}^{(m)} m^2\alpha_0^2 \mathrm{e}^{\mathrm{i}m\alpha_0\zeta}\right]. \tag{B 7}$$

Integration of (B 5) with respect to Y from $-M$ to M, followed by integration with respect to ζ from 0 to $2\pi/\alpha_0$, using the boundary conditions (B 6) while letting $M \to +\infty$, and finally integrating with respect to x_1, produces the following result for the $O(\epsilon^2)$ jump in the streamwise mean velocity:

$$\Delta U_2 = -\frac{U_c'}{U_c}\lim_{M\to+\infty}\int_{-M}^{M} Y\bar{\Omega}_1\,\mathrm{d}Y, \tag{B 8}$$

where the overbar denotes the period average. Substitution of (2.20) into (B 8), integration by parts, and using the boundary conditions for Ψ_1 leads to

$$\Delta U_2 = \frac{U_c'}{U_c}(a_2^{(0)+} - a_2^{(0)-}) - \tfrac{1}{4}|A^\dagger|^2 U_c' J_3 - \lambda^2 x_1^2 U_c' J_4. \tag{B 9}$$

Combination of (A 13) and (B 9) shows that

$$P_{2\infty}^{+} = P_{2\infty}^{-}, \tag{B 10}$$

i.e. that there is no mean pressure jump across the critical layer at $O(\epsilon^2)$.

Multiplication of (2.19) by Y, followed by integration with respect to Y from $-M$ to M, integration with respect to ζ from 0 to $2\pi/\alpha_0$, using the boundary conditions for Ψ_1 while letting $M \to +\infty$, integrating with respect to x_1, and then combining the result with (B 8), produces the additional result for the $O(\epsilon^2)$ jump in the streamwise mean velocity

$$\Delta U_2 = -\frac{\alpha_0^2 U_c'}{2U_c}|A^\dagger|^2 (J_1 - \tfrac{1}{2}U_c J_2). \tag{B 11}$$

Equations (B 10) and (B 11) can now be used to determine $a_2^{(0)+} - a_2^{(0)-}$.

Appendix C. The generic problem and large-$\lambda\bar{x}$ behaviour

The non-equilibrium nonlinear critical-layer problem, i.e. (2.39)–(2.42), can be converted into the scaled critical-layer problem for the hyperbolic-tangent mean-flow problem studied in II, by introducing the new variables and parameters (the prime does not denote differentiation in this Appendix – it is simply used to denote new quantities)

$$\bar{x}' = \int_{\bar{x}_0}^{\bar{x}} \frac{\mathrm{d}\bar{x}}{\chi^2} + \bar{x}_0' = -\tfrac{1}{2}\int_0^{x_1} \frac{\gamma S_1}{\chi^2}\mathrm{d}x_1 + \bar{x}_0', \tag{C 1}$$

$$X' = X + \int_{\bar{x}_0}^{\bar{x}} \frac{\mu}{\chi}\mathrm{d}\bar{x} + X_0' - X_0 = \alpha_0\zeta - \tfrac{1}{2}\int_0^{x_1} \frac{\mu\gamma S_1}{\chi}\mathrm{d}x_1 + X_0', \tag{C 2}$$

$$\eta' = \chi^2\eta + \chi\mu = \chi^2 \frac{\alpha_0 U_c' Y - S_1}{-\tfrac{1}{2}\bar{U}S_1} + \chi\mu, \tag{C 3}$$

$$A' = \chi^4 A \exp\left[-\mathrm{i}(X_0' - X_0) - \mathrm{i}\int_{\bar{x}_0}^{\bar{x}} \frac{\mu}{\chi}\mathrm{d}\bar{x}\right]$$

$$= \frac{\alpha_0^2 U_c' \chi^4}{(-\tfrac{1}{2}\bar{U}S_1)^2} A^\dagger \exp\left[-\mathrm{i}X_0' + \frac{\mathrm{i}}{2}\int_0^{x_1} \frac{\mu\gamma S_1}{\chi}\mathrm{d}x_1\right], \tag{C 4}$$

$$Q' = \chi^3 Q = -\frac{(\alpha_0 U_c')^2 \bar{U}\chi^3}{2U_c'''(-\tfrac{1}{2}\bar{U}S_1)^2} Q^\dagger, \tag{C 5}$$

$$\sigma' \equiv \sigma_r' + \mathrm{i}\sigma_i' = \chi\sigma - \mathrm{i}\mu = \frac{\pi}{1 + \tfrac{1}{2}\mathrm{i}\pi\bar{U}'}, \tag{C 6}$$

$$\bar{U}' = \bar{U}/\chi, \quad \bar{\lambda}' = \chi^6\bar{\lambda}, \tag{C 7), (C 8}$$

where $\bar{x}_0'$ and X_0' are determined through

$$\int_0^{\bar{x}_0'} \sigma_r' \mathrm{d}\bar{x}' = \int_0^{\bar{x}_0} \sigma_r \mathrm{d}\bar{x} + \ln\chi^4 = \ln\left[\frac{\alpha_0^2 U_c' |A_0^\dagger| \chi^4}{(-\tfrac{1}{2}\bar{U}S_1)^2}\right], \tag{C 9}$$

$$X_0' = -\int_0^{\bar{x}_0'} \sigma_i' \mathrm{d}\bar{x}' + X_0 + \int_0^{\bar{x}_0} \sigma_i \mathrm{d}\bar{x}_0 = \arg A_0^\dagger - \int_0^{\bar{x}_0'} \sigma_i' \mathrm{d}\bar{x}', \tag{C 10}$$

and with σ' replacing κ in the notation of II. Thus, the non-equilibrium nonlinear critical-layer problem studied in II, which is of the form (2.39)–(2.42) but with $\mu = 0$, applies to an arbitrary mean-flow profile provided that the meaning of $\bar{U}$ and $\bar{\lambda}$ in II are suitably generalized.

The results of II showed that, no matter what the size of the viscous parameter $\bar{\lambda}'$, the amplitude A' eventually exhibits algebraic growth as $\bar{\lambda}'\bar{x}'$ becomes large and an asymptotic solution to the non-equilibrium nonlinear critical-layer problem was constructed in that limit. This asymptotic solution is, of course, also valid in the general case analysed here and it is of the form

$$a = a_\infty \tilde{x}^{\frac{2}{3}}[1 + a_1 \tilde{x}^{-\frac{1}{6}} + a_2 \tilde{x}^{-\frac{1}{3}} + \ldots + a_6 \tilde{x}^{-1} + \ldots], \tag{C 11}$$

$$\frac{\mathrm{d}\Theta}{\mathrm{d}\bar{x}'} = \theta'_\infty[1 + \theta_1 \tilde{x}^{-\frac{1}{6}} + \theta_2 \tilde{x}^{-\frac{1}{3}} + \ldots + \theta_6 \tilde{x}^{-1} + \ldots], \tag{C 12}$$

where $\tilde{x} = \bar{\lambda}'\bar{x}', a = |A'|$, the phase Θ is defined by

$$A' = a\,\mathrm{e}^{-\mathrm{i}\Theta} \tag{C 13}$$

and $a_\infty, a_1, a_2, \ldots$ and $\theta'_\infty, \theta_1, \theta_2 \ldots$ are constants that are fully determined by the asymptotic solution without invoking any upstream matching conditions. The first few constants are given in II. Note that the asymptotic analysis only determines the phase variation (or wavenumber correction) $\mathrm{d}\Theta/\mathrm{d}\bar{x}'$ and not the phase Θ itself. This means that there is one arbitrary parameter, i.e. a constant phase factor, say Θ_0, that, in principle, can be determined by upstream matching with the numerical solution. (The asymptotic solution must be carried out to include the sixth-order terms in order to accomplish this, however.)

Appendix D. The weakly non-parallel linear stability calculation

To perform the linear and weakly non-parallel stability calculations, it turns out to be advantageous temporarily to abandon the non-dimensionalization used in the main portions of this paper. Here, the convective lengthscale $L_\omega = U_{\mathrm{A}*}/\omega_{\mathrm{e}*}$, $1/\omega_{\mathrm{e}*}$, and $U_{\mathrm{A}*}$ will be used as length, time, and velocity scales, respectively. Since the mean flow is inflexionally unstable, it follows that the frequency parameter

$$F = \omega_{\mathrm{e}*}\nu/U_{\mathrm{A}*}^2 \ll 1 \tag{D 1}$$

can be interpreted as an inverse Reynolds number, characteristic of the streamwise region in the vicinity of the linear neutral point.

A stream function for the mean flow can now be introduced in the form

$$\Psi = (2\xi)^{\frac{1}{2}} f(\xi, \eta), \tag{D 2}$$

where, now,

$$\xi = F(x + x_{\mathrm{v}}), \quad \eta = [y - y_{\mathrm{c}}(\xi)](2\xi)^{-\frac{1}{2}}; \tag{D 3), (D 4}$$

x_{v} is the distance to the virtual origin of the shear layer, and $y_{\mathrm{c}}(\xi)$ is the indeterminate location of the inflexion point. It follows that f (in the absence of any mean-flow pressure gradient) is governed by

$$f_{\eta\eta\eta} + f f_{\eta\eta} = 2\xi(f_\eta f_{\xi\eta} - f_\xi f_{\eta\eta}), \tag{D 5}$$

subject to the boundary conditions

$$f_\eta \to 1 \pm Ra \quad \text{as} \quad \eta \to \pm\infty, \quad f_{\eta\eta\eta}(\xi, 0) = 0, \tag{D 6), (D 7}$$

where $Ra = (U_1 - U_2)/(U_1 + U_2)$ is the velocity ratio of the shear layer. The introduction of the boundary condition (D 7) is allowed in view of (D 4). The ξ-dependence of f is necessary because, in general, remnants of the upstream conditions are still present and a self-similar velocity profile has not yet been achieved in the

early, i.e. linear, part of the measurement region. This is particularly so in splitter-type experiments where a substantial wake component is usually present.

The perturbation stream function is now taken to be of the form

$$\psi = \mathrm{Re}\left\{\hat{\psi}(\xi,\eta)\exp\left(\mathrm{i}\left[\frac{1}{F}\int_{\xi_e}^{\xi}\kappa(\xi)\,\mathrm{d}\xi - t\right]\right)\right\}, \tag{D 8}$$

where ξ_e is a reference location, say the excitation point, and $\hat{\psi}$ expands as

$$\hat{\psi} = A(\xi)\,\hat{\phi}(\xi,\eta) + F\hat{\psi}_1 + O(F^2). \tag{D 9}$$

Substitution of $\Psi+\psi\,(\psi \ll \Psi)$ into the Navier–Stokes equations followed by linearization with respect to the perturbation stream function and then expansion in terms of the small parameter F leads to a sequence of perturbation problems. The zeroth-order problem is simply the Rayleigh stability problem, i.e.

$$\mathscr{L}_{\mathrm{R}}\hat{\phi} = \mathrm{i}k[(U-c)(D^2-k^2) - U_{\eta\eta}]\hat{\phi} = 0, \tag{D 10}$$

subject to the boundary condition $\hat{\phi}\to 0$ as $|\eta|\to+\infty$, where $U = f_\eta$ is the streamwise mean-flow velocity, $c = 1/\kappa$, $k = (2\xi)^{\frac{1}{2}}\kappa$, and D now denotes differentiation with respect to η. The Strouhal number (of §2) based on the average velocity and the local vorticity thickness is simply $S = \delta_{\mathrm{v}}/2$, where $\delta_{\mathrm{v}} = [2Ra/\max(f_\eta)](2\xi)^{\frac{1}{2}}$ is the local (non-dimensional) vorticity thickness of the shear layer, and the streamwise wavenumber based on the local vortcity thickness is $\alpha = S\kappa$.

The solution of (D 10) subject to its boundary conditions determines the complex eigenvalue κ. The associated eigenfunction $\hat{\phi}(\xi,\eta)$ depends parametrically on ξ through the coefficients in (D 10) and the factor $A(\xi)$ in (D 9) is an amplitude function which is determined by a secularity condition for the next-order (i.e. $O(F)$) problem. That problem reads

$$\mathscr{L}_{\mathrm{R}}\hat{\psi}_1 = -(2\xi)^{\frac{1}{2}}[a(\hat{\phi})A' + b(\hat{\phi})A], \tag{D 11}$$

where

$$a = (2k^2c - 3k^2f_\eta - f_{\eta\eta\eta})\hat{\phi} + f_\eta \mathrm{D}^2\hat{\phi}, \tag{D 12}$$

$$\begin{aligned} b = {} & (2k^2c - 3k^2f_\eta - f_{\eta\eta\eta})\left(\frac{\partial\hat{\phi}}{\partial\xi} - \frac{\eta}{2\xi}\mathrm{D}\hat{\phi}\right) + f_\eta\left(\frac{\partial \mathrm{D}^2\hat{\phi}}{\partial\xi} - \frac{\eta}{2\xi}\mathrm{D}^3\hat{\phi} - \frac{1}{\xi}\mathrm{D}^2\hat{\phi}\right) \\ & + k(c-3f_\eta)\left(\frac{\partial k}{\partial\xi} - \frac{k}{2\xi}\right)\hat{\phi} - \frac{1}{2\xi}[(f_{\eta\eta} + \eta f_{\eta\eta\eta} - 2\xi f_{\eta\eta\xi})\mathrm{D}\hat{\phi} \\ & + (f - \eta f_\eta + 2\xi f_\xi)(\mathrm{D}^2-k^2)\mathrm{D}\hat{\phi}] + 2k^2(f_\eta - c)\frac{y_c'}{(2\xi)^{\frac{1}{2}}}\mathrm{D}\hat{\phi} - \frac{1}{2\xi}(\mathrm{D}^2-k^2)^2\hat{\phi}. \end{aligned} \tag{D 13}$$

The boundary conditions for (D 11) are that $\hat{\psi}_1\to 0$ as $|\eta|\to+\infty$. The factor a is identical to and, excluding the last two terms, b reduces for self-similar mean flows (i.e. $f_\xi \equiv 0$) to the corresponding results in Gaster's (1974) investigation on the effects of boundary-layer growth of flow stability. The second-to-last term in b arises because of (D 4), i.e. the indeterminate location of the inflexion point, and the last term is the viscous term. In studies dealing with flows, such as a Blasius boundary layer, where the instability is caused by viscous effects, that last term, of course, cannot be treated as a higher-order term – it must be included heuristically in the zeroth-order equation, thus, leading to the Orr–Sommerfeld rather than the Rayleigh stability problem. However, the viscous term is a correction term of the same order of magnitude as the non-parallel mean-flow effects for inviscidly unstable flows (Lanchon & Eckhaus 1964). For brief discussions of weakly non-parallel

theories, the reader is referred to Drazin & Reid (1982, p. 479) for the case of (wall) boundary-layer flows and to the survey paper by Ho & Huerre (1984) for the particular application to unbounded shear flow. The viscous term was ignored in the shear-layer investigations described in the latter reference.

The solvability condition, or Fredholm alternative, for (D 11) gives

$$\frac{A'}{A} \equiv \mathrm{i}\kappa_1 = -\int_{-\infty}^{+\infty} \frac{\hat{\phi} b(\hat{\phi})}{U-c}\,\mathrm{d}\eta \Big/ \int_{-\infty}^{+\infty} \frac{\hat{\phi} a(\hat{\phi})}{U-c}\,\mathrm{d}\eta, \tag{D 14}$$

where κ_1 can be interpreted as a local $O(F)$ wavenumber correction. As can easily be seen by inspection, the second-to-last term in b (cf. (D 13)) does not contribute in (D 14). Thus, as can be expected, a transverse shift in the mean streamwise velocity profile does not affect the linear stability problem neither to leading order nor in the correction for weak mean-flow divergence. (The boundary condition (D 7) can then be exchanged with a more expedient condition from a computational point of view – the one actually used in this investigation was to prescribe f as $\eta \to \infty$.)

The derivatives with respect to ξ of k and the eigenfunction $\hat{\phi}$ that are needed in the evaluation of b can be obtained either by the numerical differentiation of the results obtained for different ξ or by the procedure first suggested by Saric & Nayfeh (1975). In this latter procedure (D 10) is differentiated with respect to ξ to yield

$$\mathscr{L}_{\mathrm{R}} \frac{\partial \hat{\phi}}{\partial \xi} = \mathrm{i}k\left[g(\hat{\phi})\frac{\partial k}{\partial \xi} - h(\hat{\phi})\right], \tag{D 15}$$

subject to $\partial\hat{\phi}/\partial\xi \to 0$ as $|\eta| \to +\infty$, where

$$g = 2k(f_\eta - c)\,\hat{\phi} - \frac{c}{k}(\mathrm{D}^2 - k^2)\,\phi, \tag{D 16}$$

$$h = \left(f_{\eta\xi} - \frac{c}{2\xi}\right)(\mathrm{D}^2 - k^2)\,\hat{\phi} - f_{\eta\eta\eta\xi}\hat{\phi}. \tag{D 17}$$

The solvability condition for (D 15) gives

$$\frac{\partial k}{\partial \xi} = \int_{-\infty}^{+\infty} \frac{\hat{\phi} h(\hat{\phi})}{U-c}\,\mathrm{d}\eta \Big/ \int_{-\infty}^{+\infty} \frac{\hat{\phi} g(\hat{\phi})}{U-c}\,\mathrm{d}\eta, \tag{D 18}$$

and (D 15) can then be solved for $\partial\hat{\phi}/\partial\xi$. Both techniques were actually used here as an internal check of the accuracy of the calculations.

The undisturbed mean-flow problem was integrated numerically by using central-difference approximations for the η-derivatives, an implicit second-order scheme to march the solution forward in ξ, and Newton iteration to solve the resulting nonlinear difference equations for each successive streamwise step. As the mean-flow solution was marched forward, the local linear eigenvalue and eigenfunction were determined using a shooting technique incorporating a forth-order Adams implicit method to integrate the local linear stability equation, and the weakly non-parallel eigenvalue correction was then calculated.

REFERENCES

Benney, D. J. & Bergeron, R. F. 1969 A new class of non-linear waves in parallel flows. *Stud. Appl. Maths* **48**, 181–204.

Drazin, P. G. & Reid, W. H. 1982 *Hydrodynamic Stability*. Cambridge University Press.

DRUBKA, R. E. 1981 Instabilities in near fields of turbulent jets and their dependence on initial conditions and Reynolds number. Ph.D. thesis, Dept. Mechanical and Aerospace Engineering, Illinois Institute of Technology, Chicago.

FREYMUTH, P. 1966 On transition in a separated laminar boundary layer. *J. Fluid Mech.* **25**, 683–704.

GASTER, M. 1974 On the effects of boundary-layer growth on flow stability. *J. Fluid Mech.* **66**, 465–480.

GOLDSTEIN, M. E. & HULTGREN, L. S. 1988 Nonlinear spatial evolution of an externally excited instability wave in a free shear layer. *J. Fluid Mech.* **197**, 295–330 (referred to herein as II).

GOLDSTEIN, M. E. & LEIB, S. J. 1988 Nonlinear roll-up of externally excited free shear layers. *J. Fluid Mech.* **191**, 481–515 (referred to herein as I).

HO, C.-M. & HUERRE, P. 1984 Perturbed free shear layers. *Ann. Rev. Fluid Mech.* **16**, 365–424.

HUANG, L.-S. & HO, C.-M. 1990 Small-scale transition in a plane mixing layer. *J. Fluid Mech.* **210**, 475–500.

LANCHON, H. & ECKHAUS, W. 1964 Sur l'analyse de la stabilité des écoulements faiblement divergent. *J. Méc.* **3**, 445–459.

LEIB, S. J. & GOLDSTEIN, M. E. 1989 Nonlinear interaction between the sinuous and varicose instability modes in a plane wake. *Phys. Fluids* A **1**, 513–521.

MONKEWITZ, P. A. & HUERRE, P. 1982 Influence of the velocity ratio on the spatial instability of mixing layers. *Phys. Fluids* **25**, 1137–1143.

SARIC, W. S. & NAYFEH, A. H. 1975 Nonparallel stability of boundary layers. *Phys. Fluids* **18**, 945–950.

THOMAS, F. O. & CHU, H. C. 1989 An experimental investigation of the transition of a planar jet: subharmonic suppression and upstream feedback. *Phys. Fluids* A **1**, 1566–1587.

VAN DYKE, M. 1975 *Perturbation Methods in Fluid Mechanics*. Parabolic.

YIH, C.-S. 1969 *Fluid Mechanics*. McGraw-Hill.